Supplementary Information for "Identification of deficiencies in seasonal rainfall simulated by CMIP5 climate models"

Caroline M. Dunning[1], Richard P. Allan[1,2,3], and Emily Black [1,2]

1. Department of Meteorology, University of Reading, Reading, UK.
2. NCAS-Climate, University of Reading, Reading, UK.
3. National Centre for Earth Observation (NCEO)

Corresponding author: C. M. Dunning, Department of Meteorology, University of Reading, Whiteknights, Reading, UK.
(c.m.dunning@pgr.reading.ac.uk)

This Supplementary Information includes the individual plots for the individual models. This document contains Figures S1 to S26, and Tables S1 to S2.

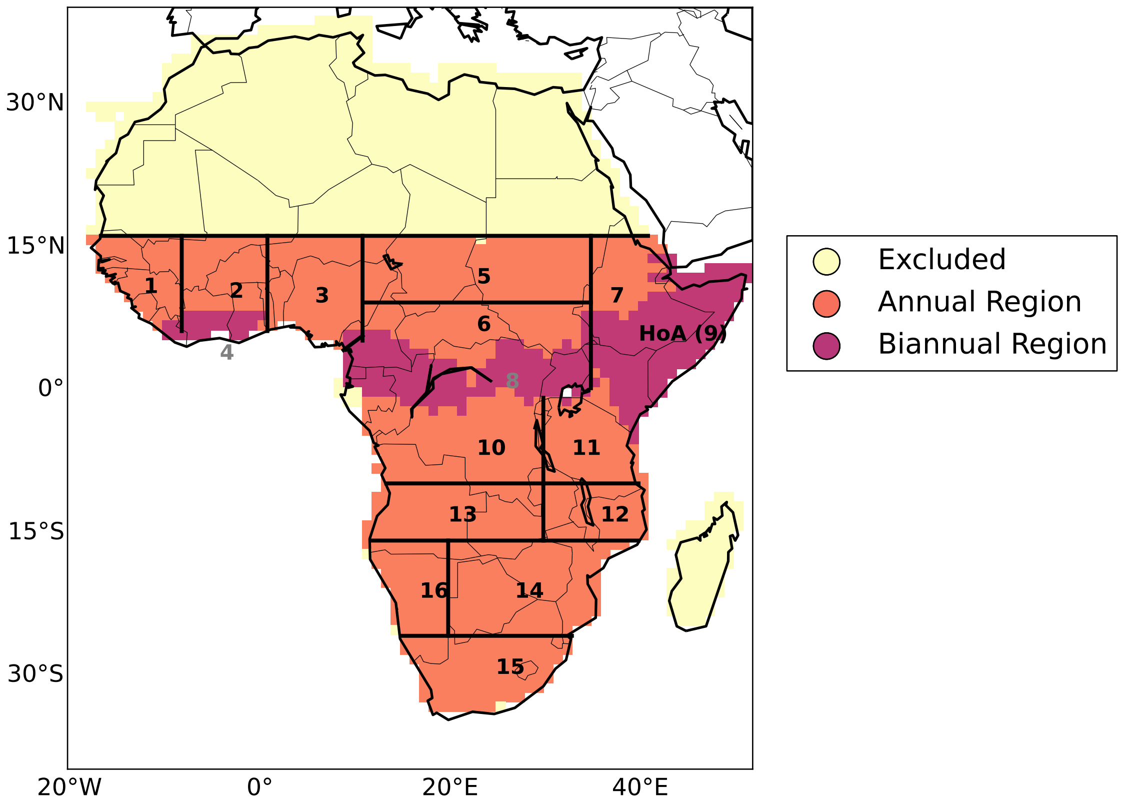

Figure S1: Regions used for analysis of seasonal timing (1-16). Yellow indicates areas excluded, pink indicates biannual regime and orange indicates regions with an annual regime. Region 4 is referred to in the text as South West Africa Coastline (SWAC). Region 8 (grey number) was not analysed, due to large observational disparities.

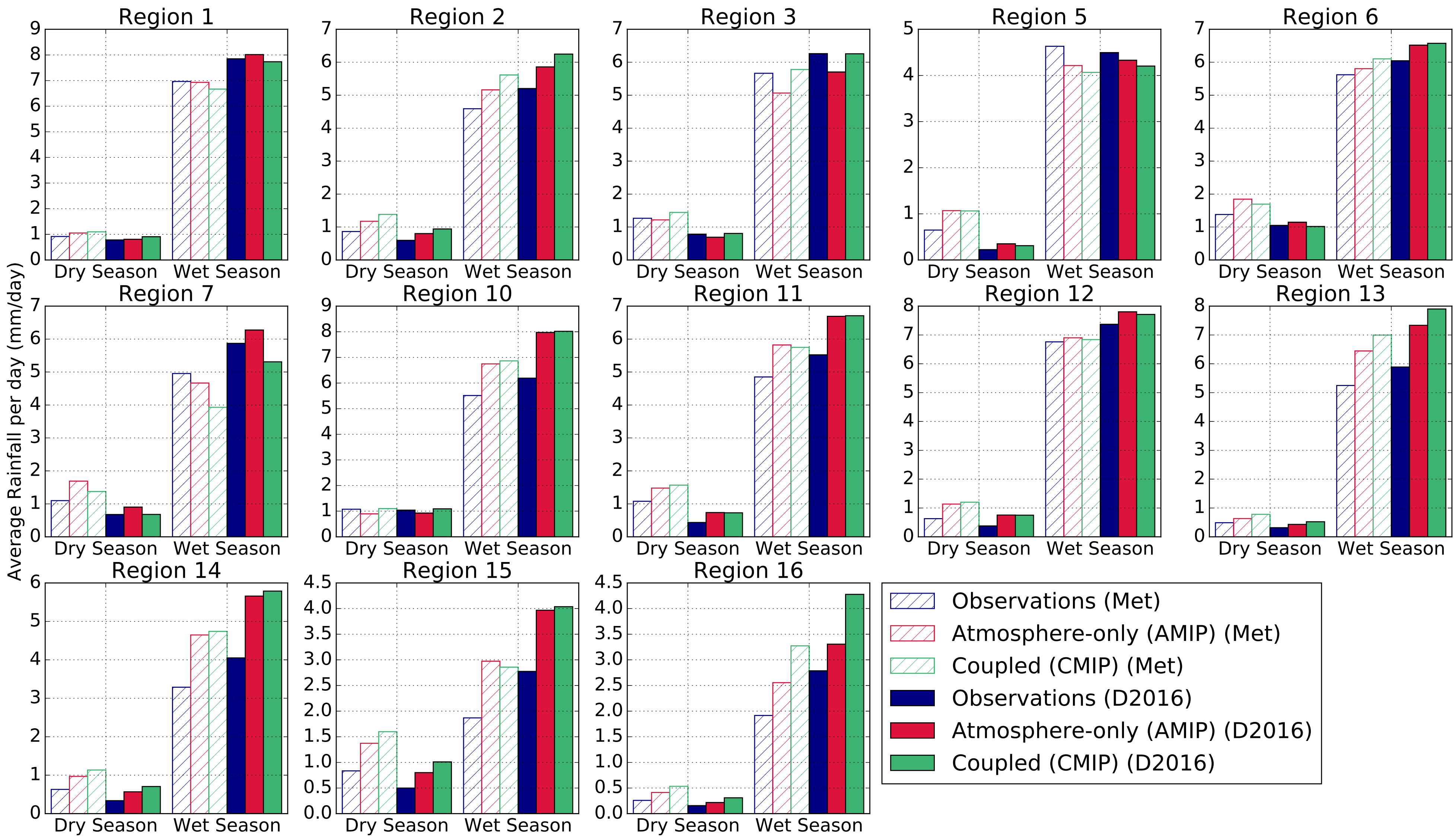

Figure S2: Average rainfall rate (mm/day) during the wet and dry seasons over annual regime regions when defined using meteorological seasons (dashed bars) and dynamically varying seasons ((*Dunning et al.*, 2016), solid). Long term means were computed for each model/dataset; the multi-model mean is plotted here. Meteorological wet seasons are June-October (Region 1), May-September (Region 2,3), July-September (Region 5), June-September (Region 7), May-October (Region 6), October-April (Region 10), December-March (Region 11,12,16), November-March (Region 13), and November-February (Region 14,15).

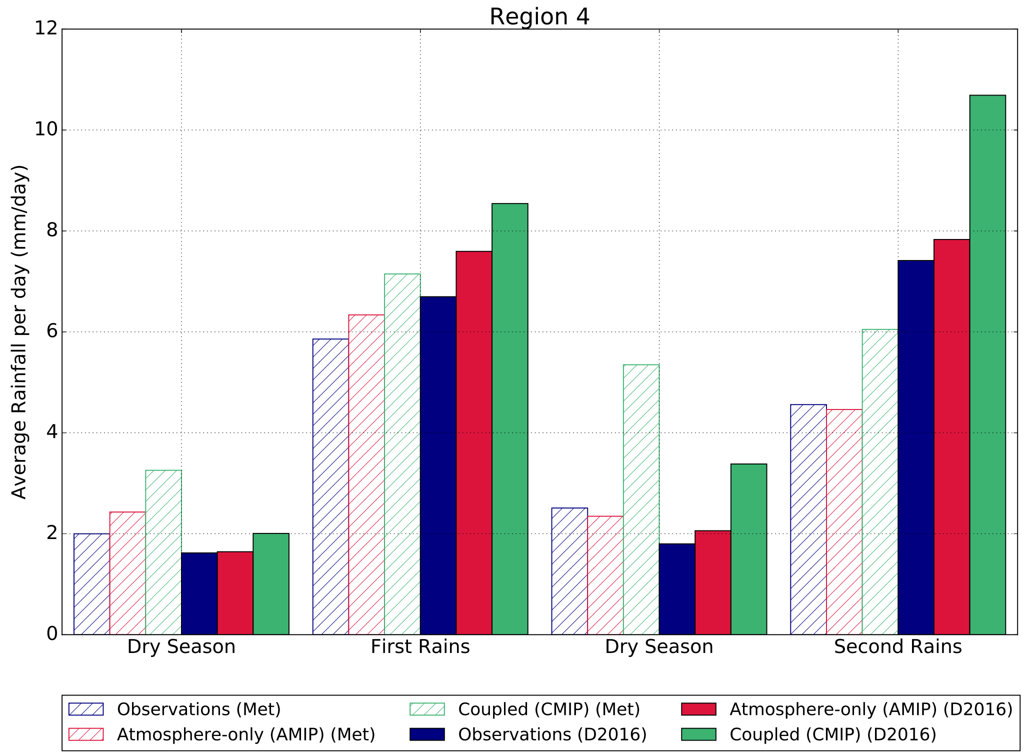

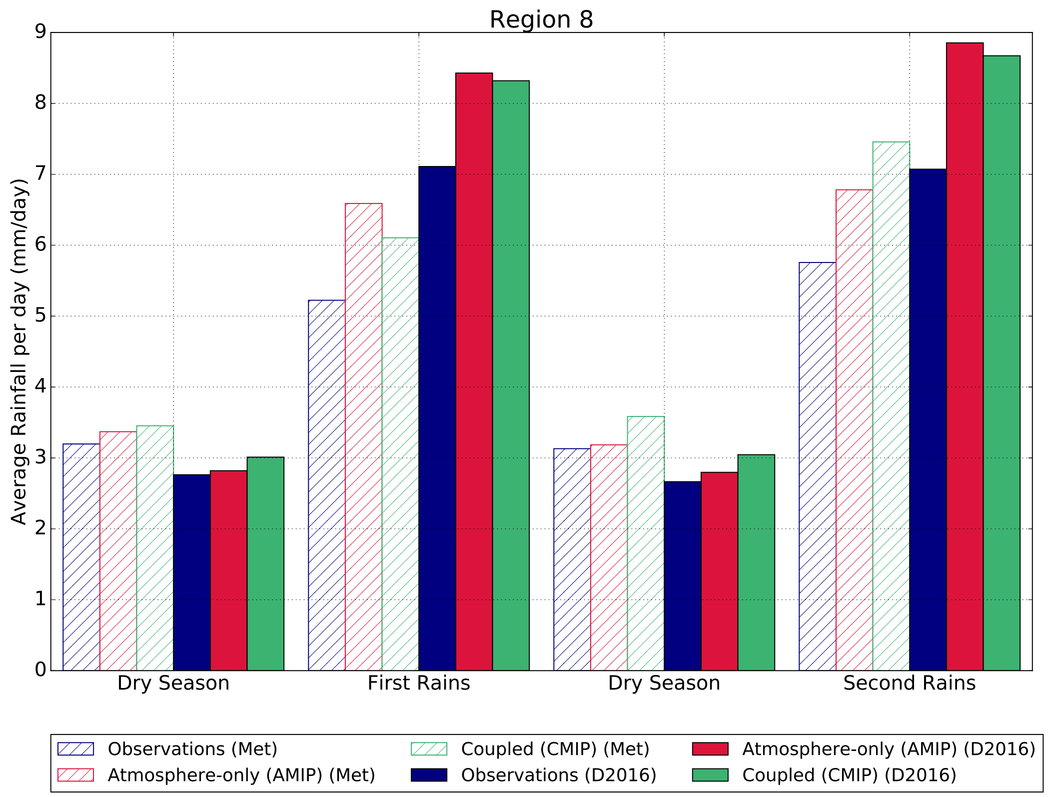

Figure S3: Average rainfall rate (mm/day) during the wet and dry seasons over biannual regime regions when defined using meteorological seasons (dashed bars) and dynamically varying seasons ((*Dunning et al.*, 2016), solid). Long term means were computed for each model/dataset; the multi-model mean is plotted here. Over the southern West African Coastline (region 4; top) the wet seasons are April-June (first rains) and September-October (second rains). Over Central Africa (region 8; bottom) the wet seasons are March-May (first rains) and September-November (second rains). The plots for the Horn of Africa (region 9) and the Sahel are included in the main paper (Figure 1).

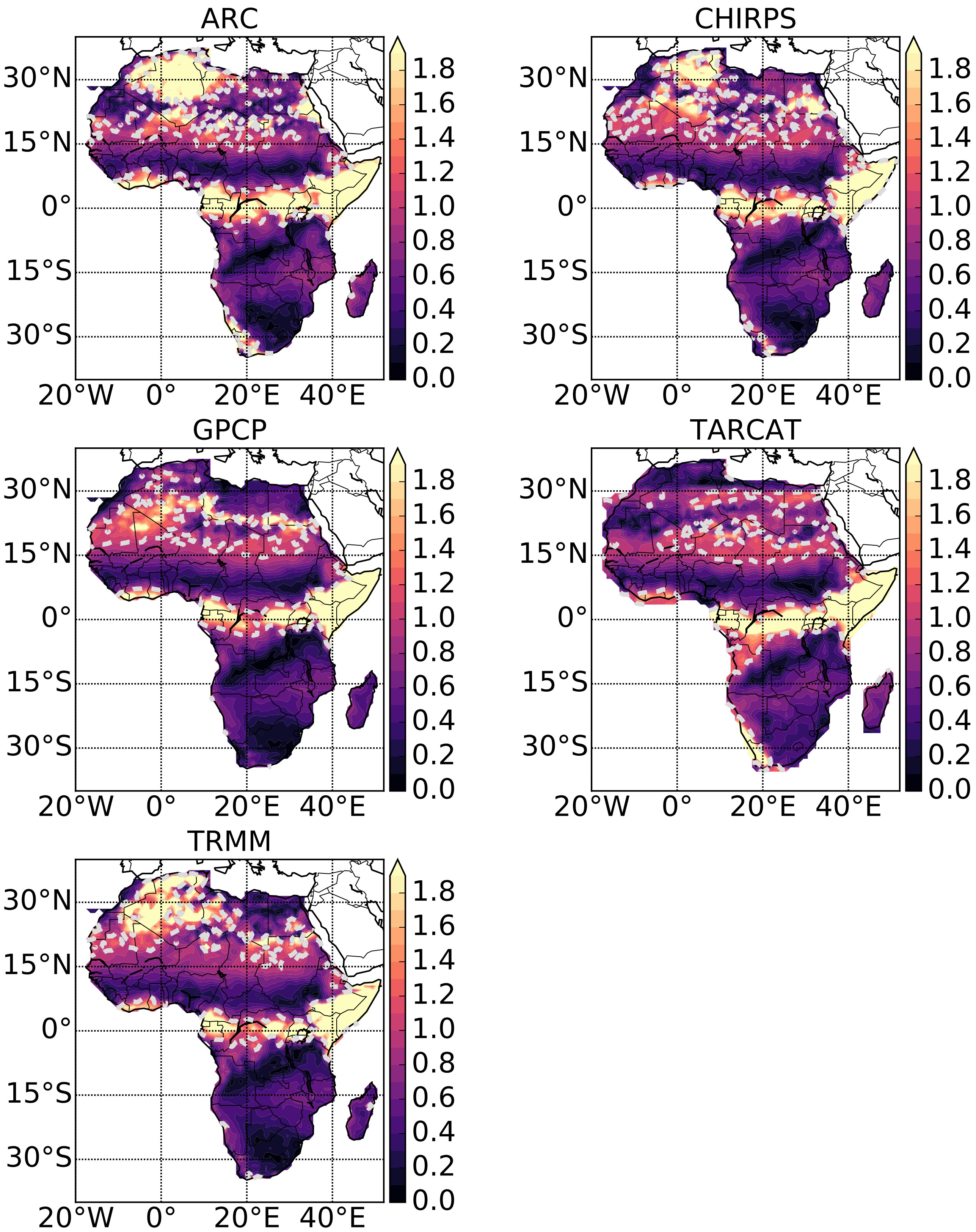

Figure S4: The ratio of the amplitude of the harmonic at two cycles per year to the amplitude of the harmonic at one cycle per year for each observational dataset used (Table S2). The dashed contour marks where the ratio is equal to 1.0.

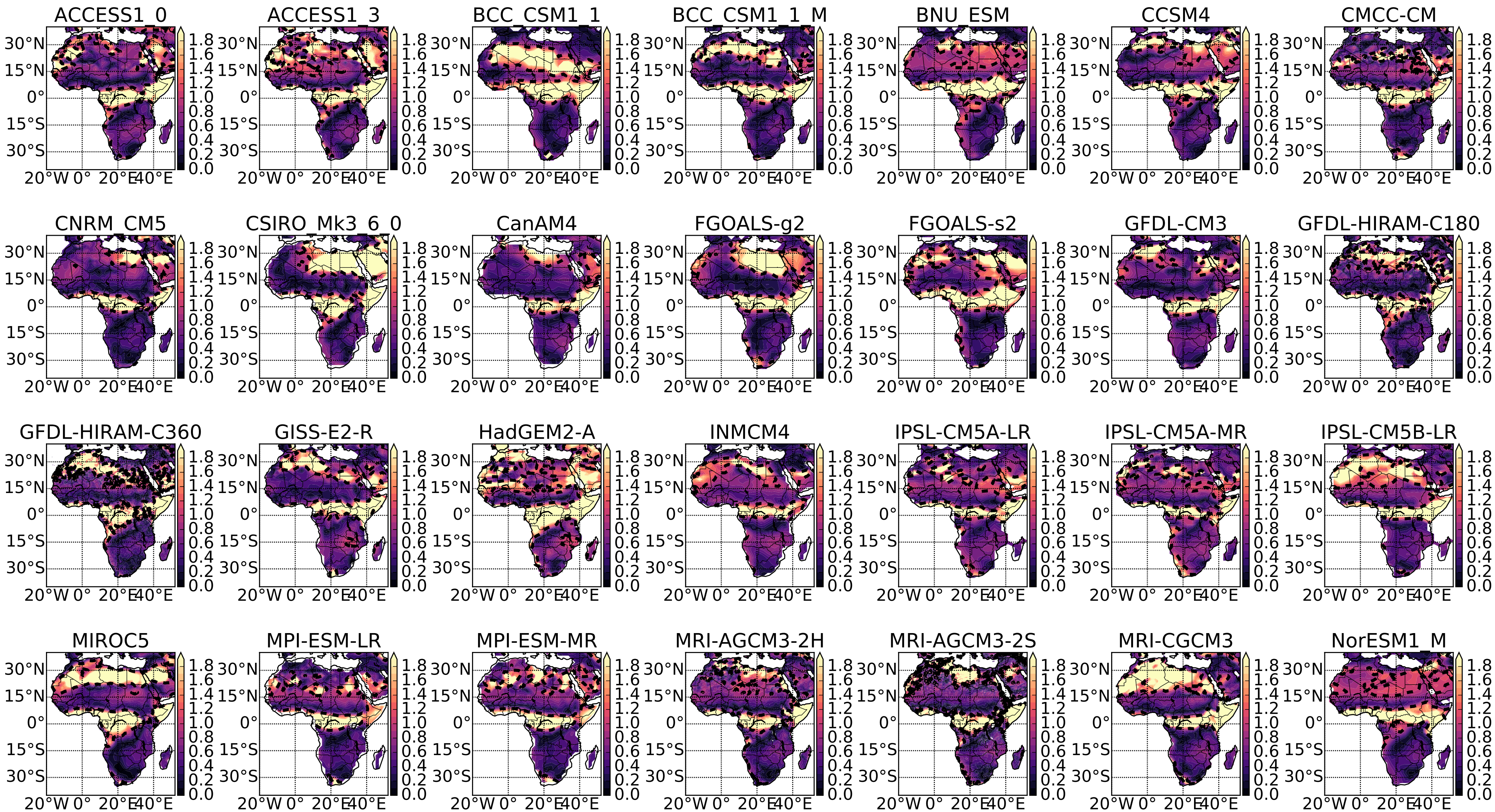

Figure S5: The ratio of the amplitude of the harmonic at two cycles per year to the amplitude of the harmonic at one cycle per year for each AMIP simulation used (Table S1). The dashed contour marks where the ratio is equal to 1.0.

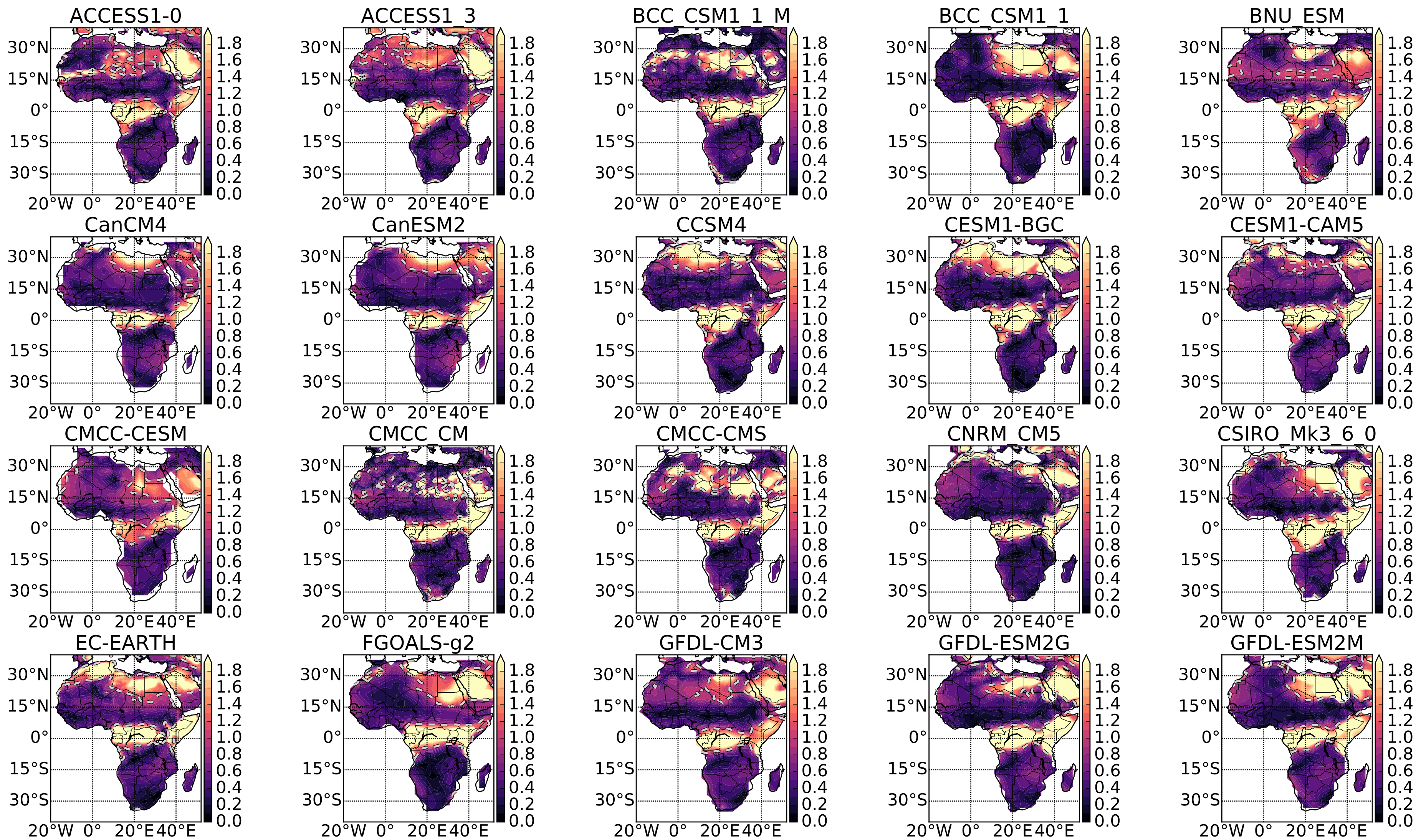

Figure S6: The ratio of the amplitude of the harmonic at two cycles per year to the amplitude of the harmonic at one cycle per year for half of the CMIP historical simulations used (Table S1, other half in Figure S7). The dashed contour marks where the ratio is equal to 1.0.

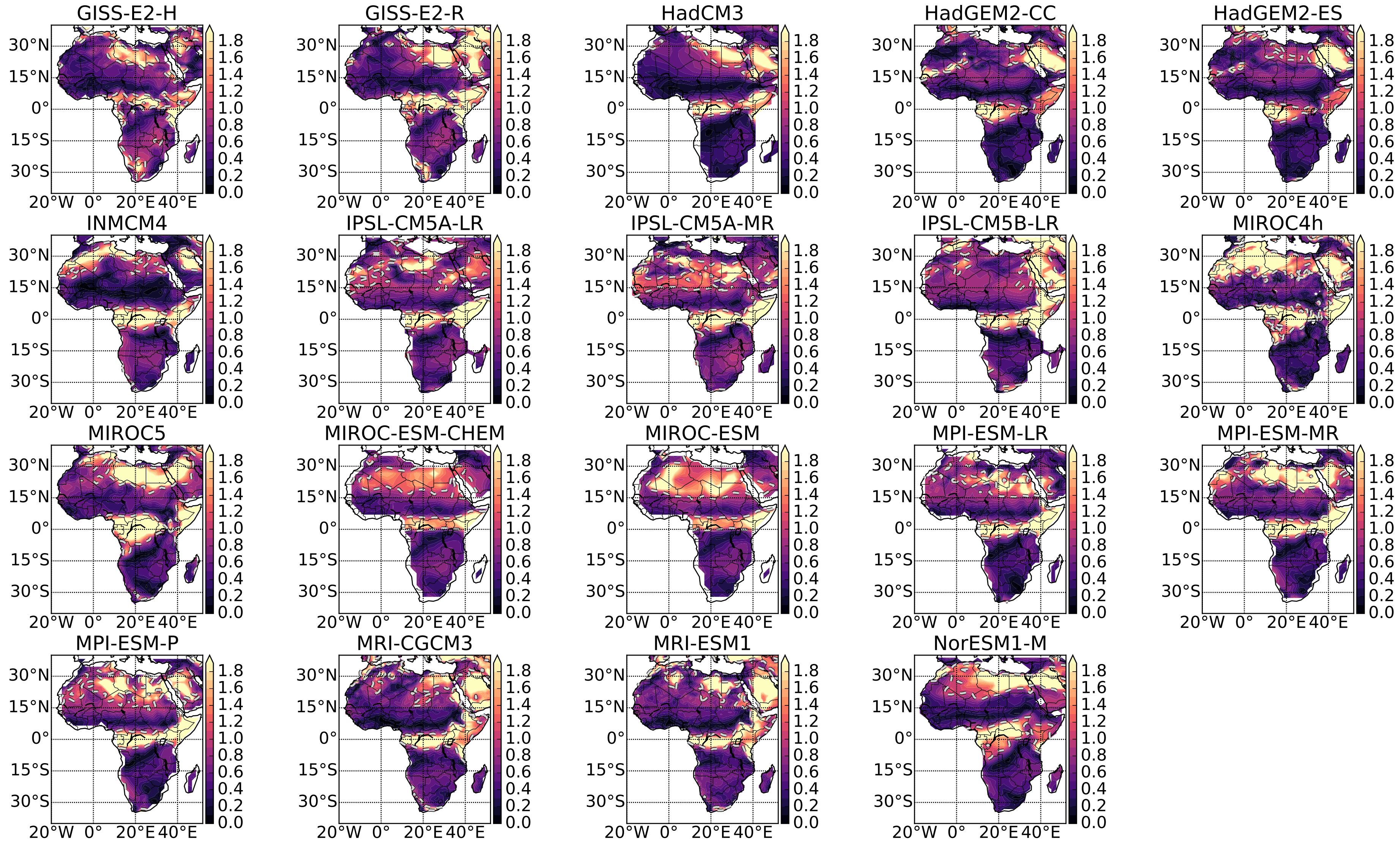

Figure S7: The ratio of the amplitude of the harmonic at two cycles per year to the amplitude of the harmonic at one cycle per year for half of the CMIP historical simulations used (Table S1, other half in Figure S6). The dashed contour marks where the ratio is equal to 1.0.

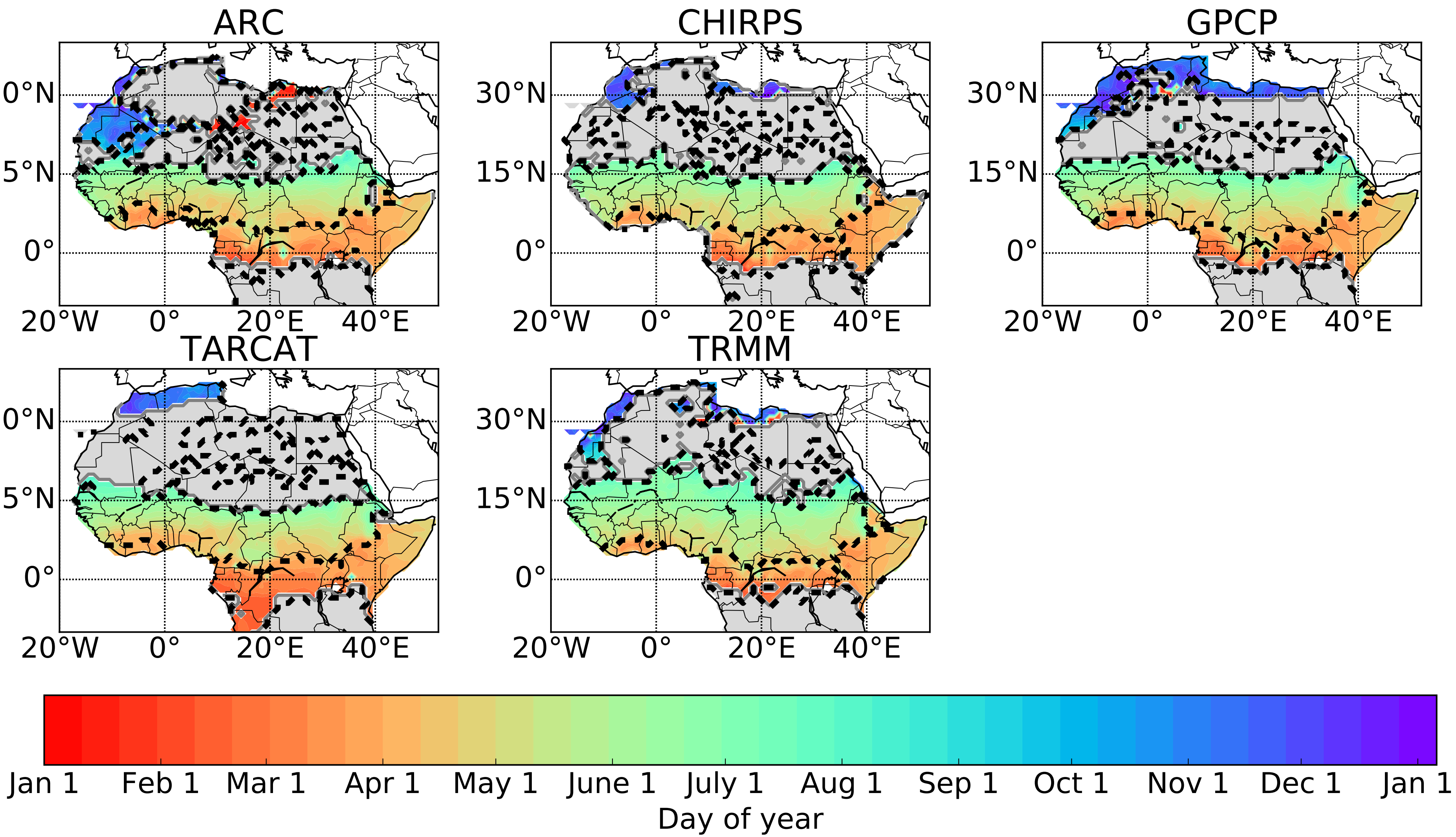

Figure S8: Seasonal progression of the onset/cessation of wet seasons in each of the observational datasets used (Table S2). The northward progression of onset in boreal spring from first/long rains over the biannual region into West African Monsoon (WAM) is shown. The dashed black line shows the annual/biannual boundaries. Grey indicates regions not considered for these plots.

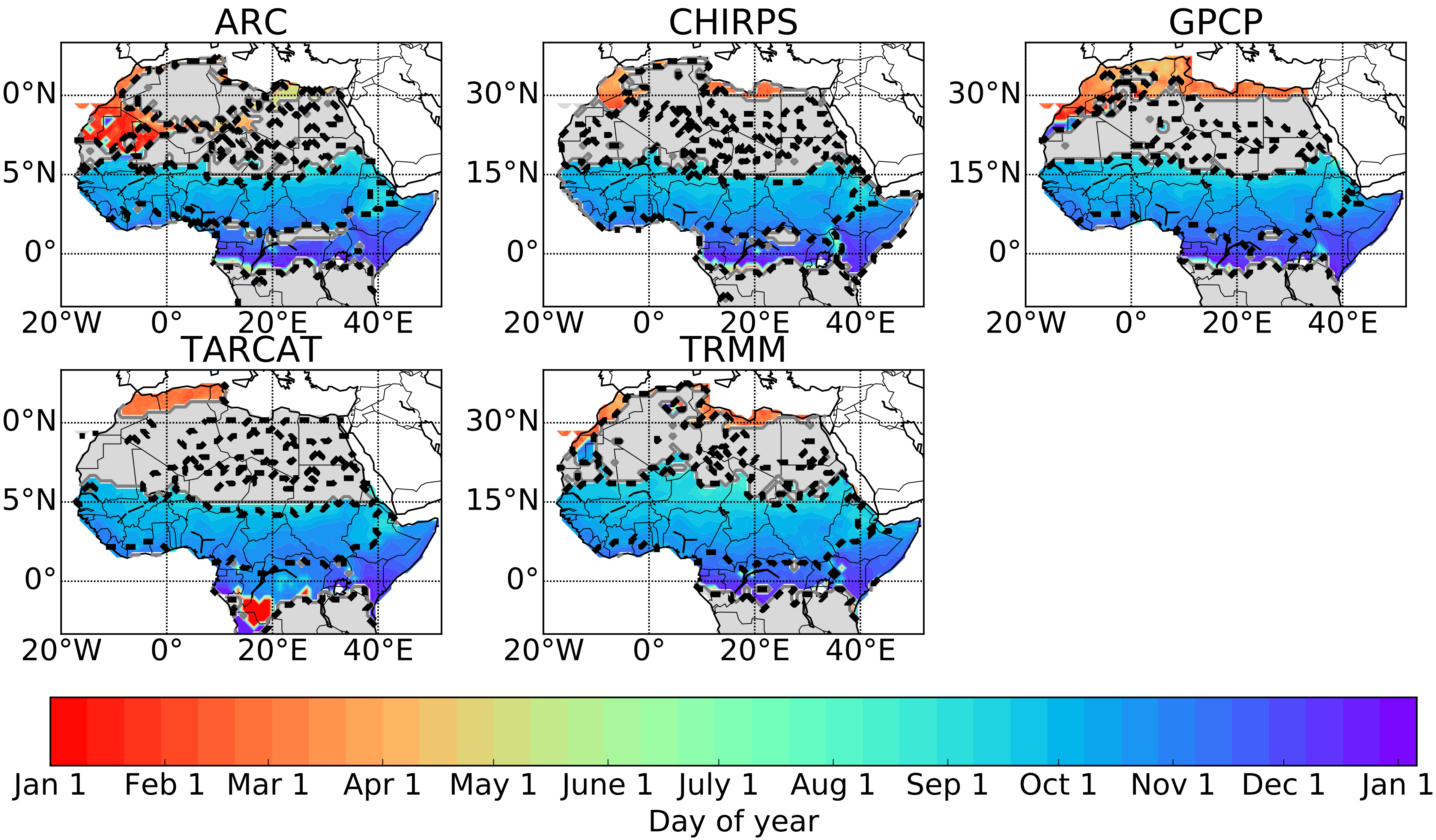

Figure S9: Seasonal progression of the onset/cessation of wet seasons in each of the observational datasets used (Table S2). Here, the southward progression of cessation in boreal autumn from the West African Monsoon into the end of the second/short rains is plotted. The dashed black line shows the annual/biannual boundaries. Grey indicates regions not considered for these plots.

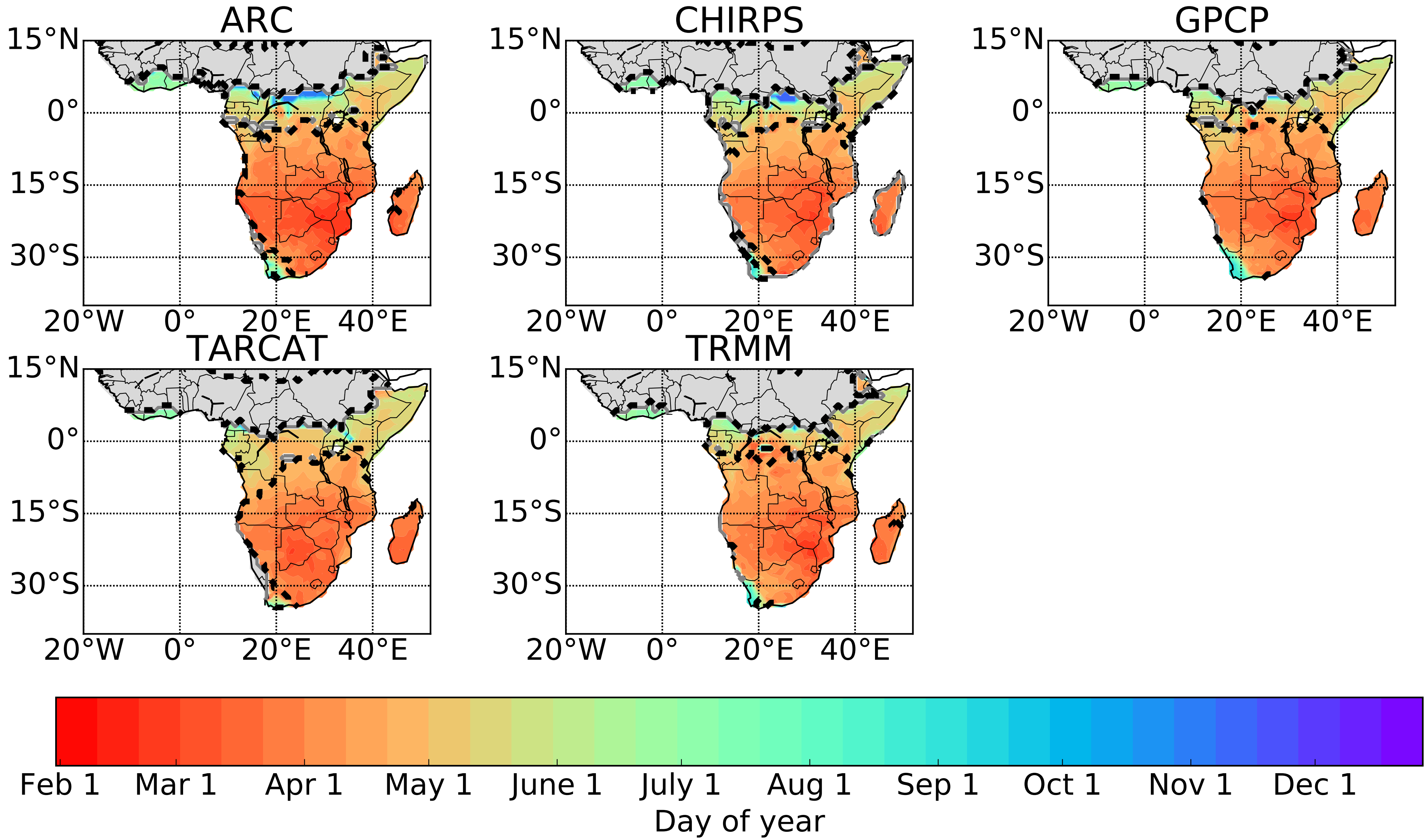

Figure S10: Seasonal progression of the onset/cessation of wet seasons in each of the observational datasets used (Table S2). This plot shows the northward progression of cessation in boreal spring from the end of the annual rains over southern Africa into the first/long rains over then biannual regime region. The dashed black line shows the annual/biannual boundaries. Grey indicates regions not considered for these plots.

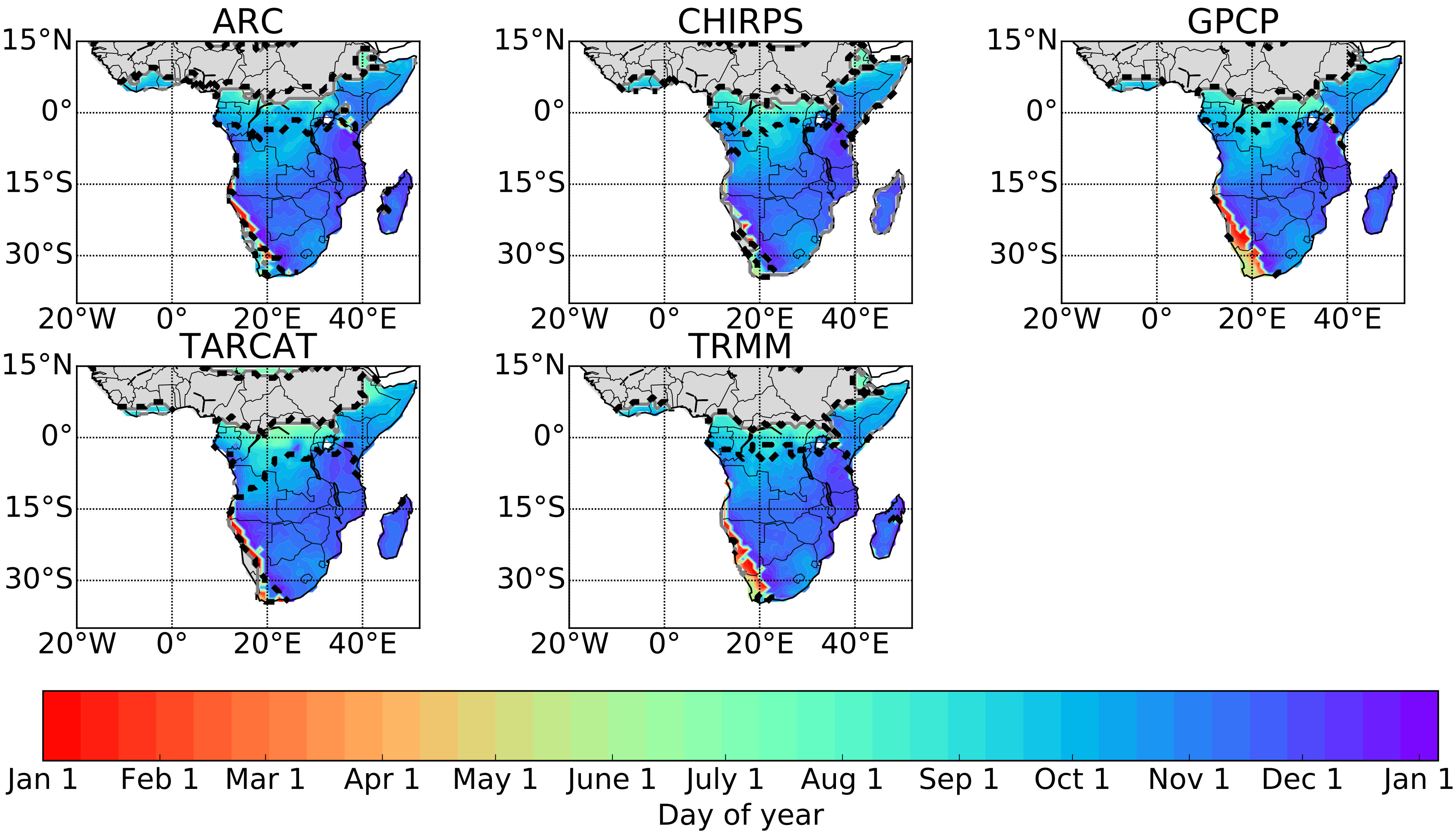

Figure S11: Seasonal progression of the onset/cessation of wet seasons in each of the observational datasets used (Table S2). The southward progression of onset in boreal autumn is plotted, from the second/short rains over the biannual region into the annual rains over southern Africa. The dashed black line shows the annual/biannual boundaries. Grey indicates regions not considered for these plots.

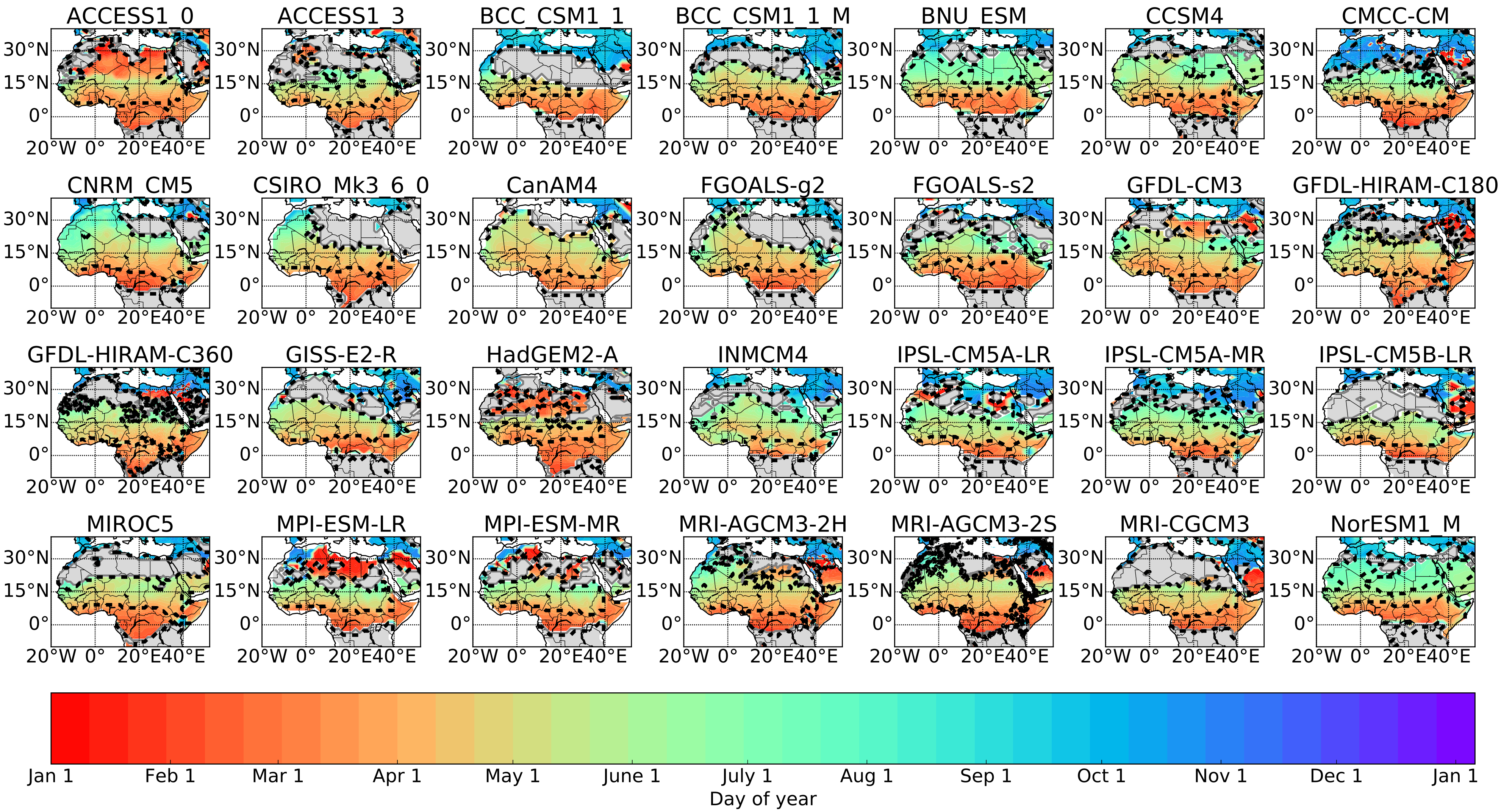

Figure S12: Seasonal progression of the onset/cessation of wet seasons in each of the AMIP simulations used (Table S1). The northward progression of onset in boreal spring from first/long rains over the biannual region into West African Monsoon (WAM) is shown. The dashed black line shows the annual/biannual boundaries. Grey indicates regions not considered for these plots.

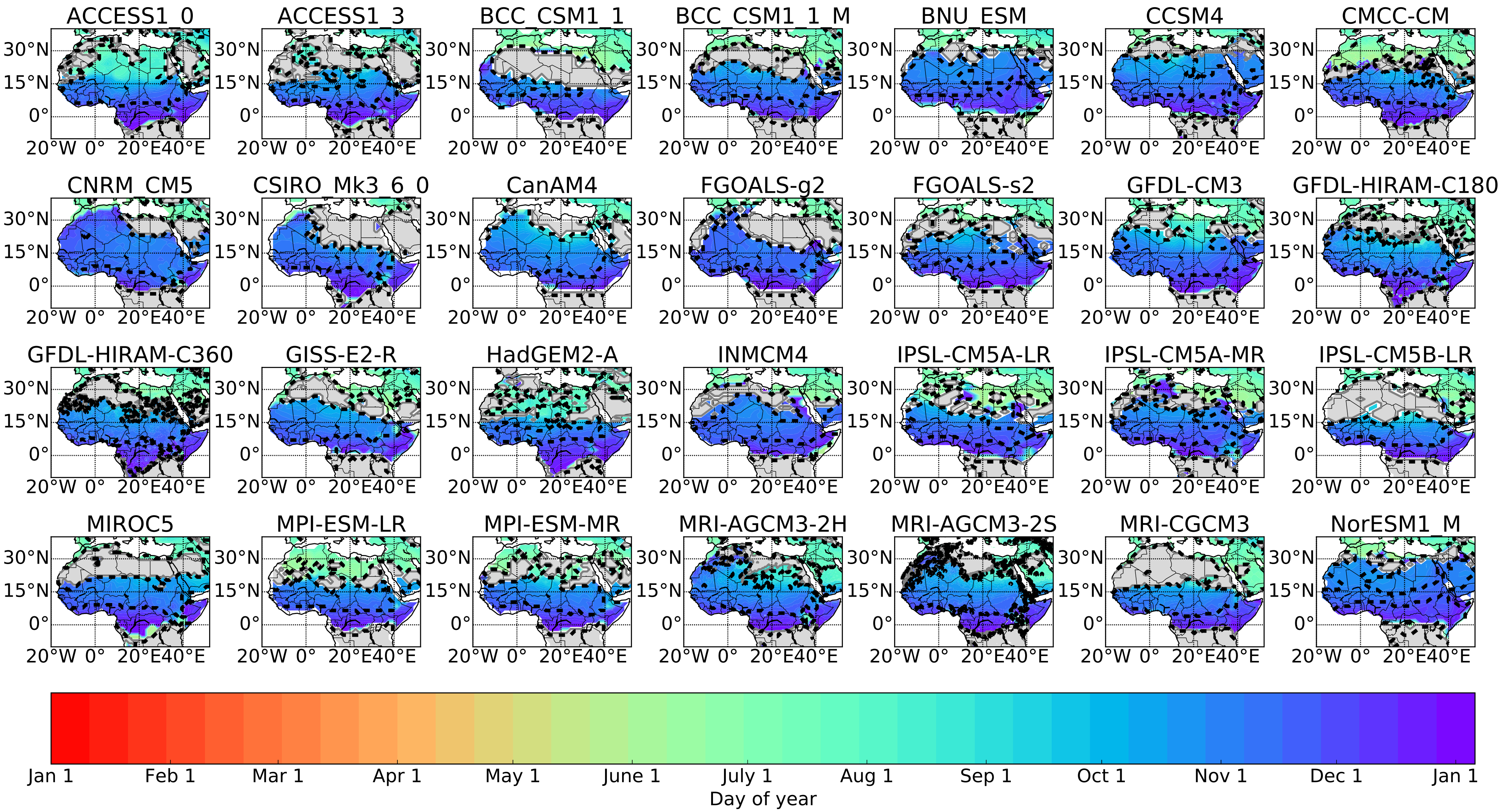

Figure S13: Seasonal progression of the onset/cessation of wet seasons in each of the AMIP simulations used (Table S1). Here, the southward progression of cessation in boreal autumn from the West African Monsoon into the end of the second/short rains is plotted. The dashed black line shows the annual/biannual boundaries. Grey indicates regions not considered for these plots.

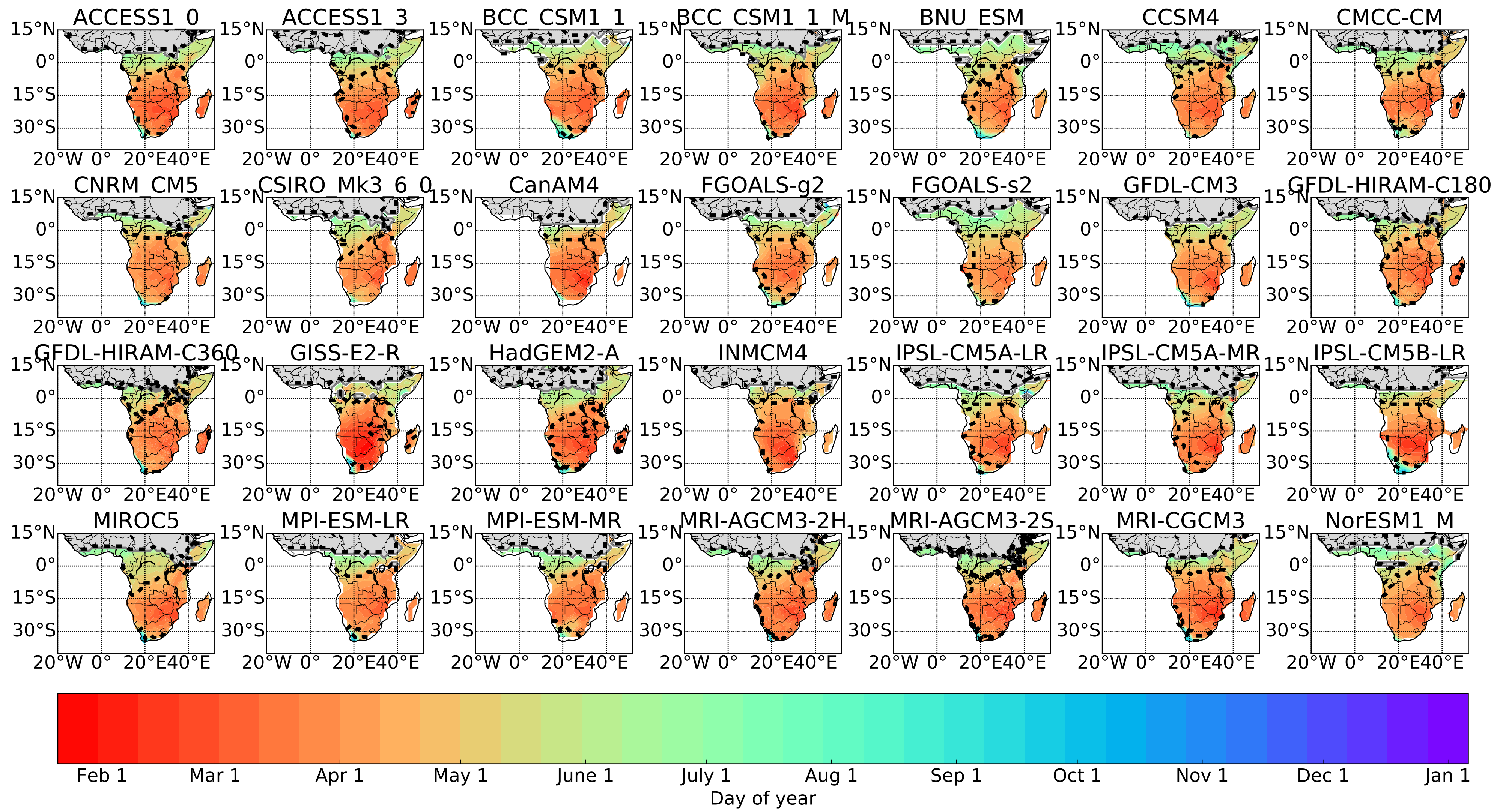

Figure S14: Seasonal progression of the onset/cessation of wet seasons in each of the AMIP simulations used (Table S1). This plot shows the northward progression of cessation in boreal spring from the end of the annual rains over southern Africa into the first/long rains over then biannual regime region. The dashed black line shows the annual/biannual boundaries. Grey indicates regions not considered for these plots.

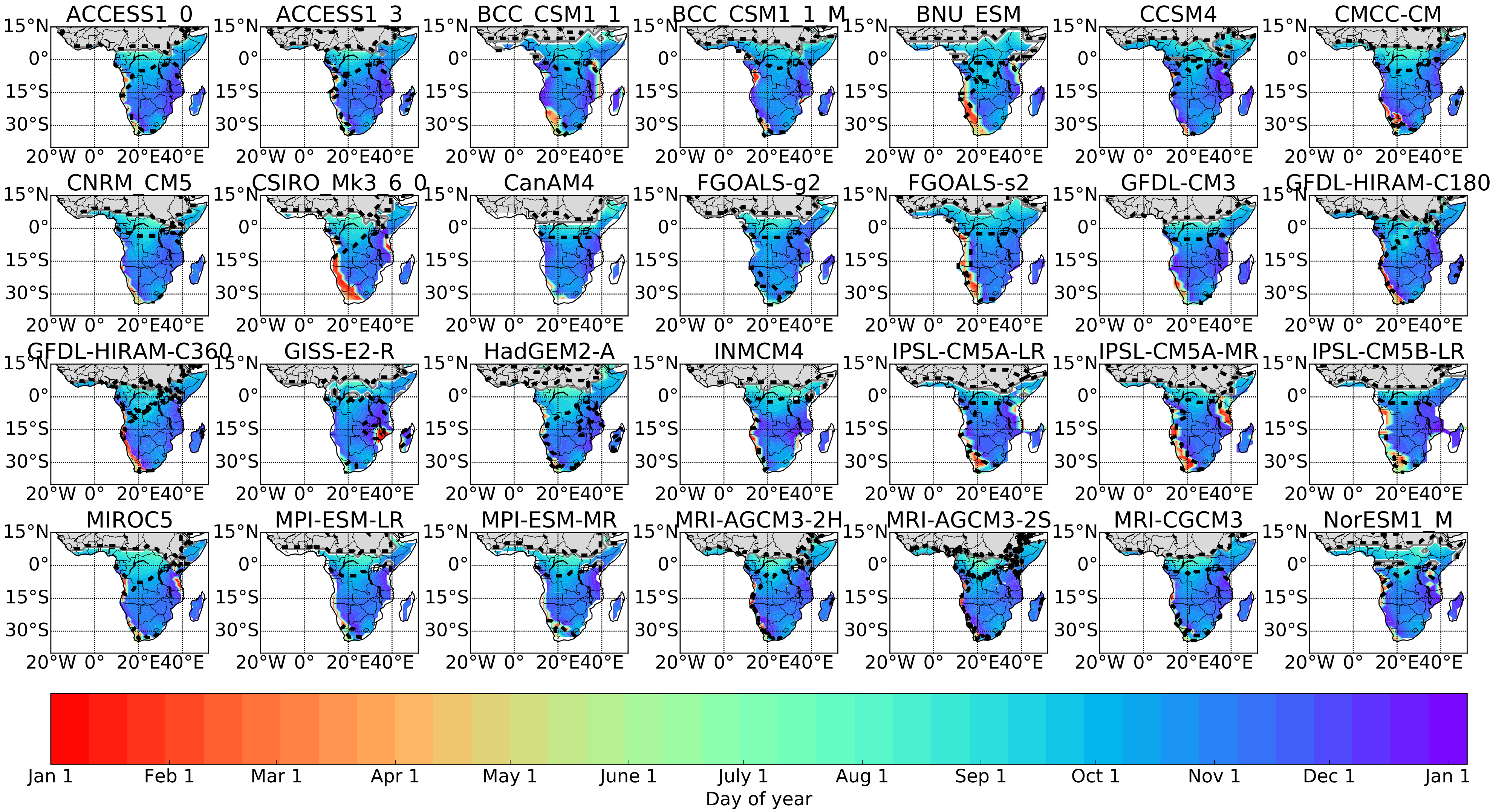

Figure S15: Seasonal progression of the onset/cessation of wet seasons in each of the AMIP simulations used (Table S1). The southward progression of onset in boreal autumn is plotted, from the second/short rains over the biannual region into the annual rains over southern Africa. The dashed black line shows the annual/biannual boundaries. Grey indicates regions not considered for these plots.

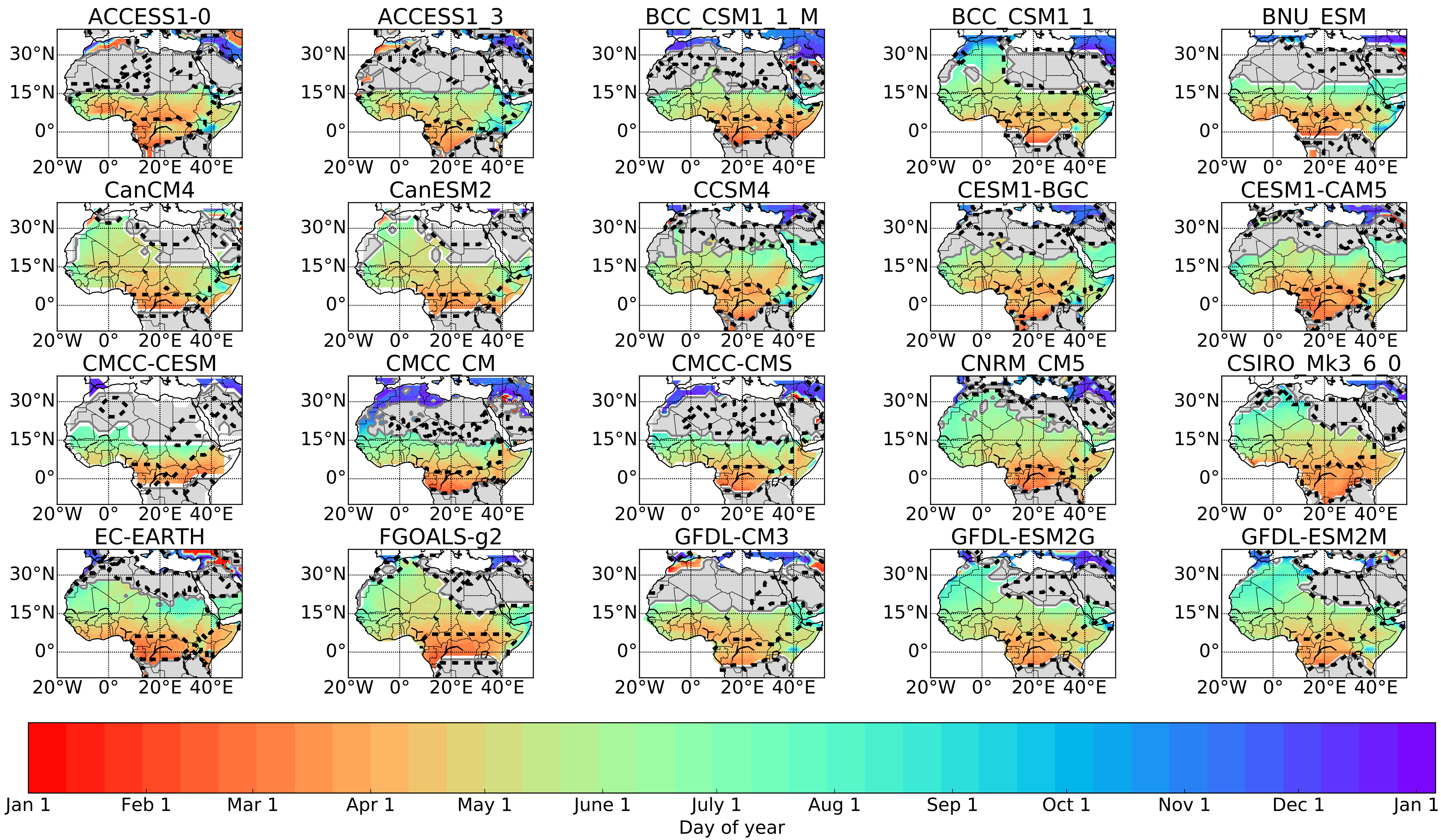

Figure S16: Seasonal progression of the onset/cessation of wet seasons in first half (alphabetical, second half in Figure S17) of the CMIP simulations used (Table S1). The northward progression of onset in boreal spring from first/long rains over the biannual region into West African Monsoon (WAM) is shown. The dashed black line shows the annual/biannual boundaries. Grey indicates regions not considered for these plots.

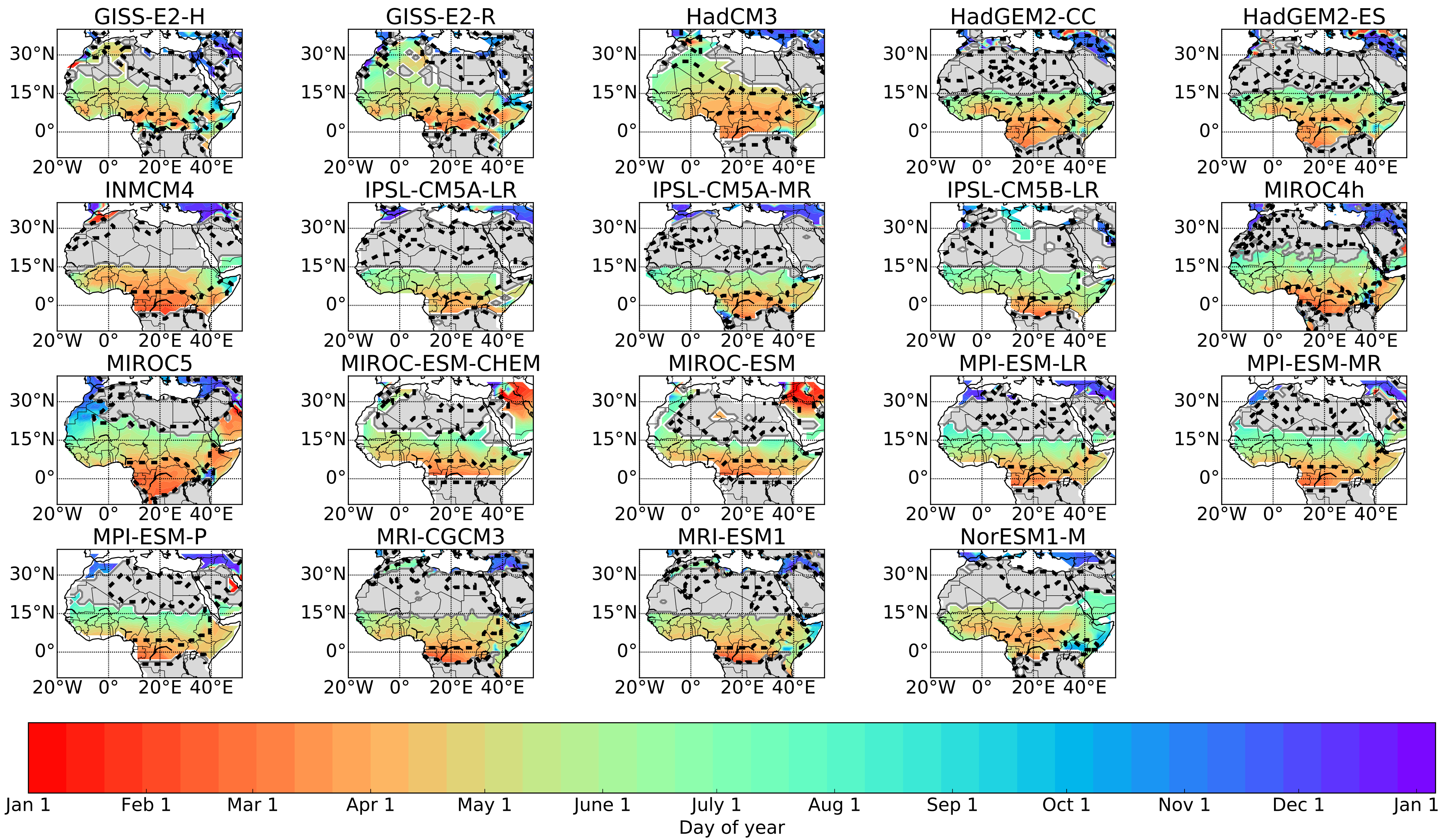

Figure S17: Seasonal progression of the onset/cessation of wet seasons in second half (alphabetical, first half in Figure S16) of the CMIP simulations used (Table S1). The northward progression of onset in boreal spring from first/long rains over the biannual region into West African Monsoon (WAM) is shown. The dashed black line shows the annual/biannual boundaries. Grey indicates regions not considered for these plots.

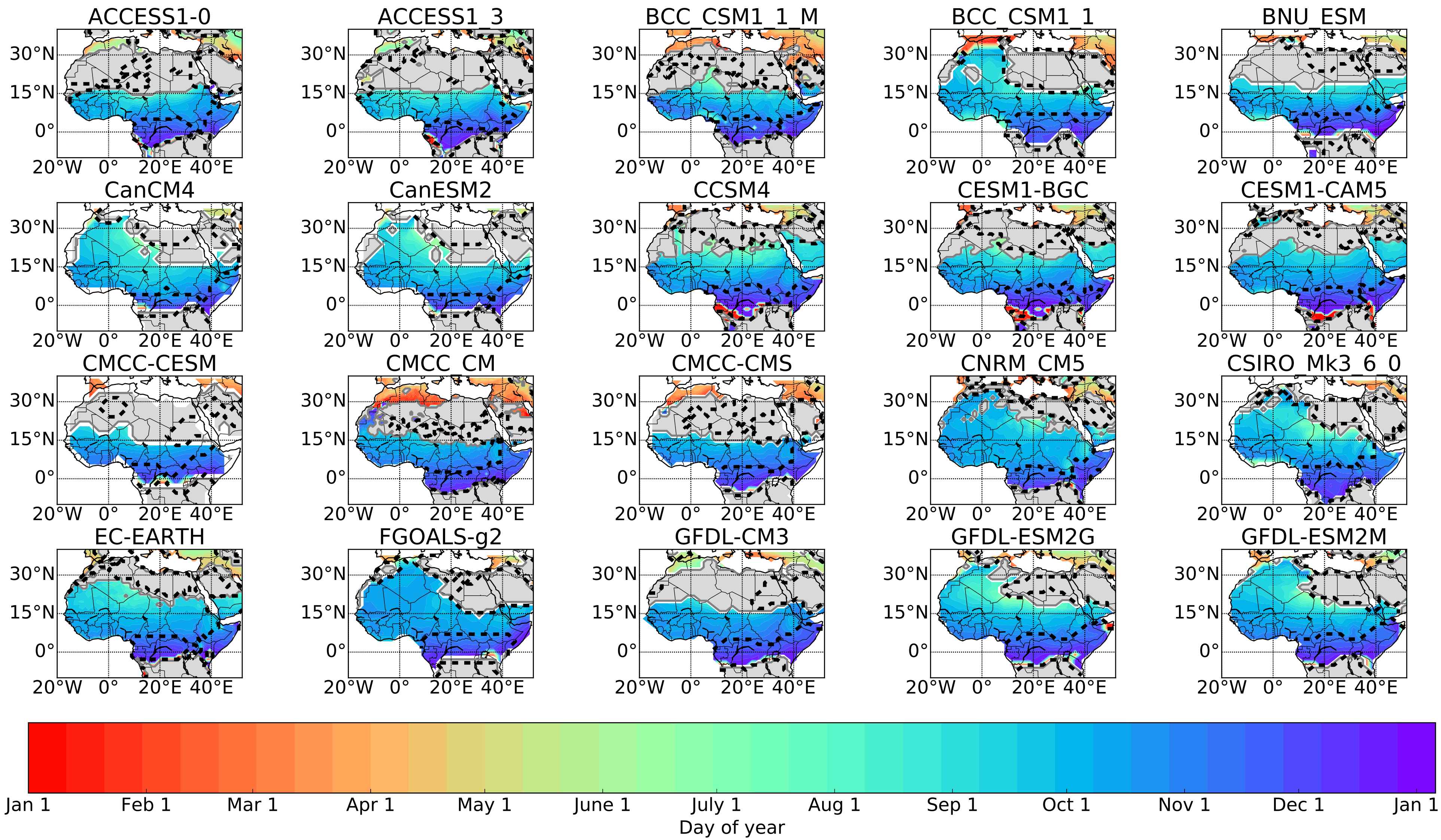

Figure S18: Seasonal progression of the onset/cessation of wet seasons in first half (alphabetical, second half in Fig S19) of the CMIP simulations used (Table S1). Here, the southward progression of cessation in boreal autumn from the West African Monsoon into the end of the second/short rains is plotted. The dashed black line shows the annual/biannual boundaries. Grey indicates regions not considered for these plots.

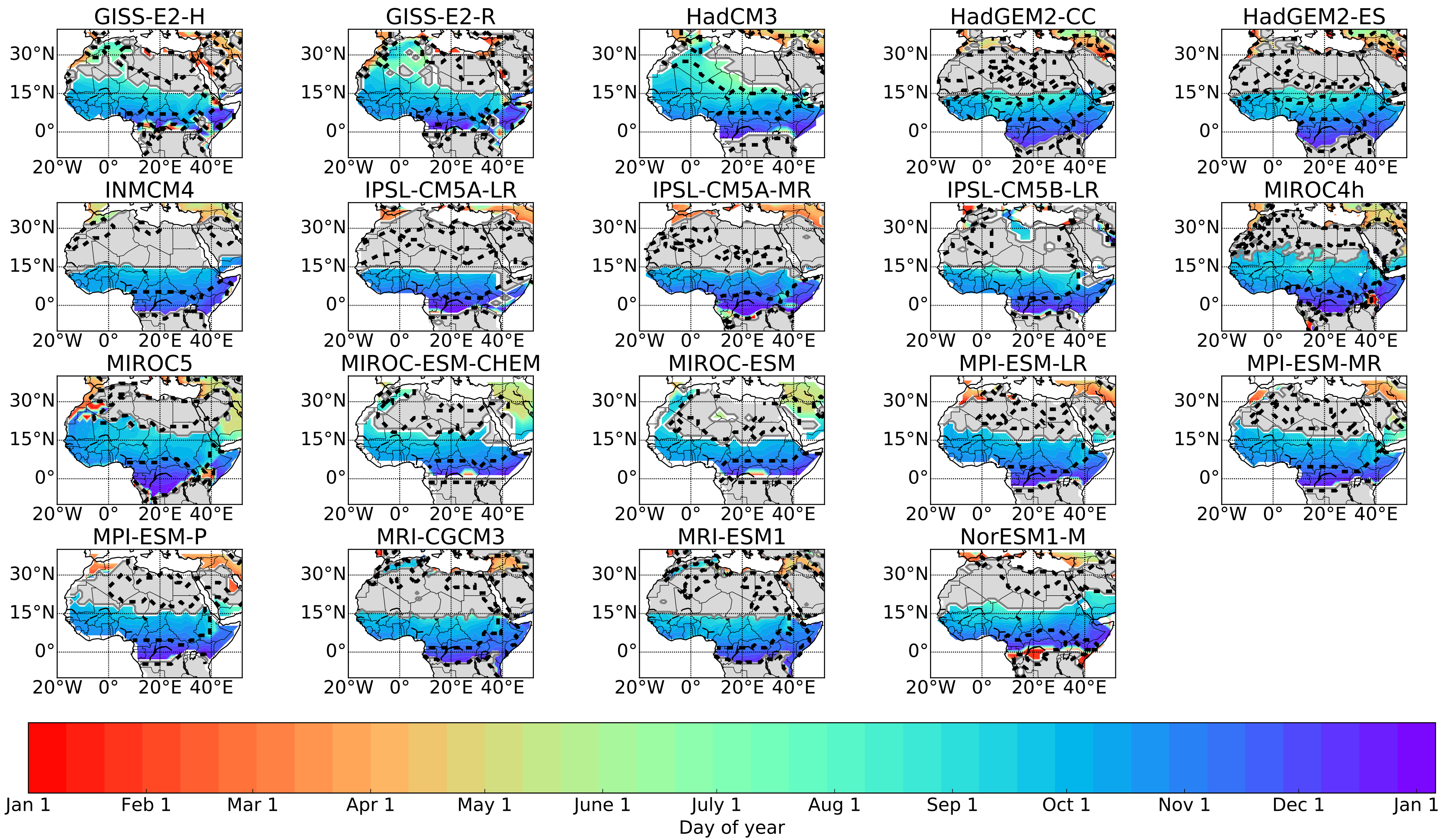

Figure S19: Seasonal progression of the onset/cessation of wet seasons in second half (alphabetical, first half in Fig S18) of the CMIP simulations used (Table S1). Here, the southward progression of cessation in boreal autumn from the West African Monsoon into the end of the second/short rains is plotted. The dashed black line shows the annual/biannual boundaries. Grey indicates regions not considered for these plots.

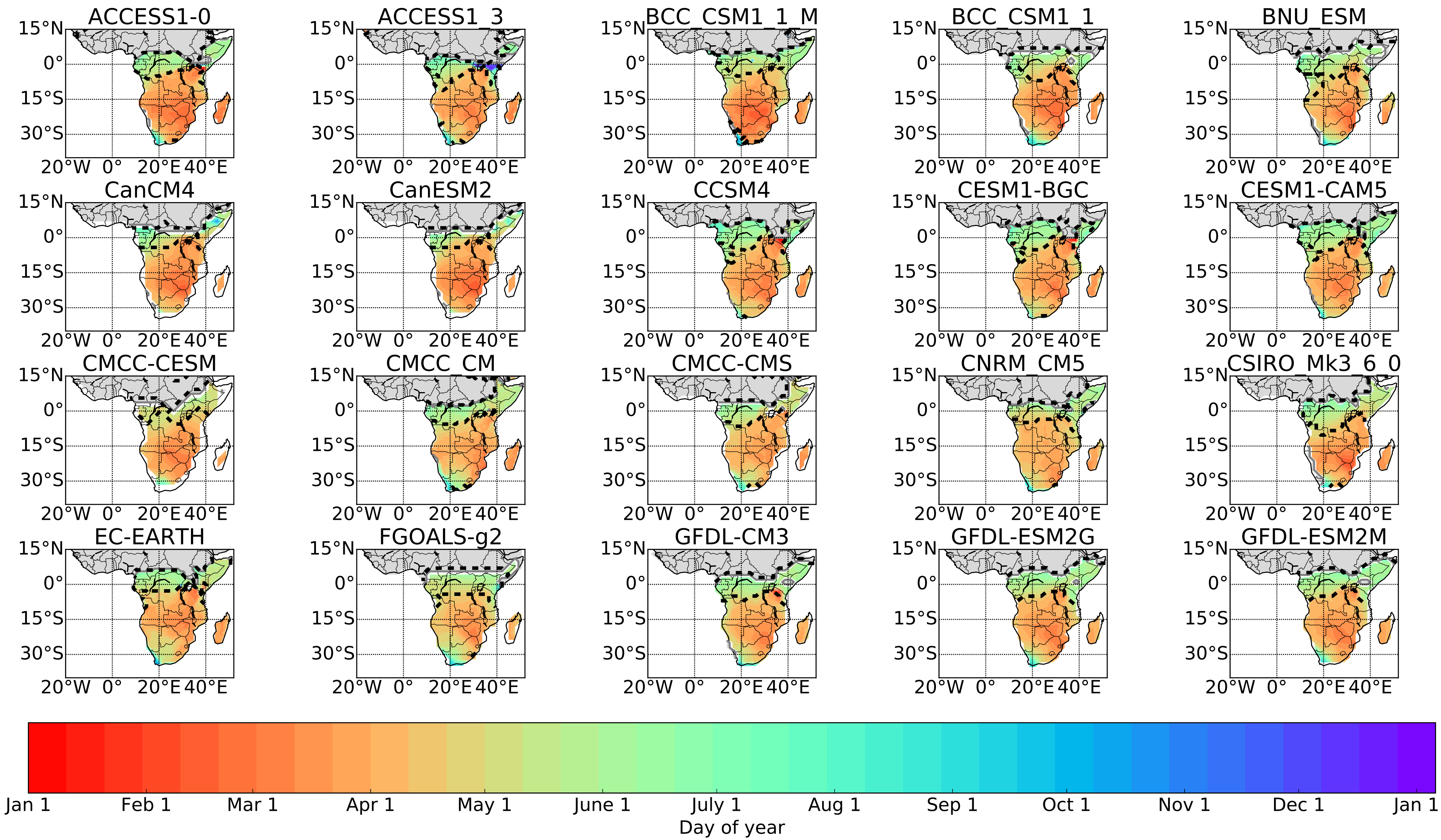

Figure S20: Seasonal progression of the onset/cessation of wet seasons in first half (alphabetical, second half in Fig S21) of the CMIP simulations used (Table S1). This plot shows the northward progression of cessation in boreal spring from the end of the annual rains over southern Africa into the first/long rains over then biannual regime region. The dashed black line shows the annual/biannual boundaries. Grey indicates regions not considered for these plots.

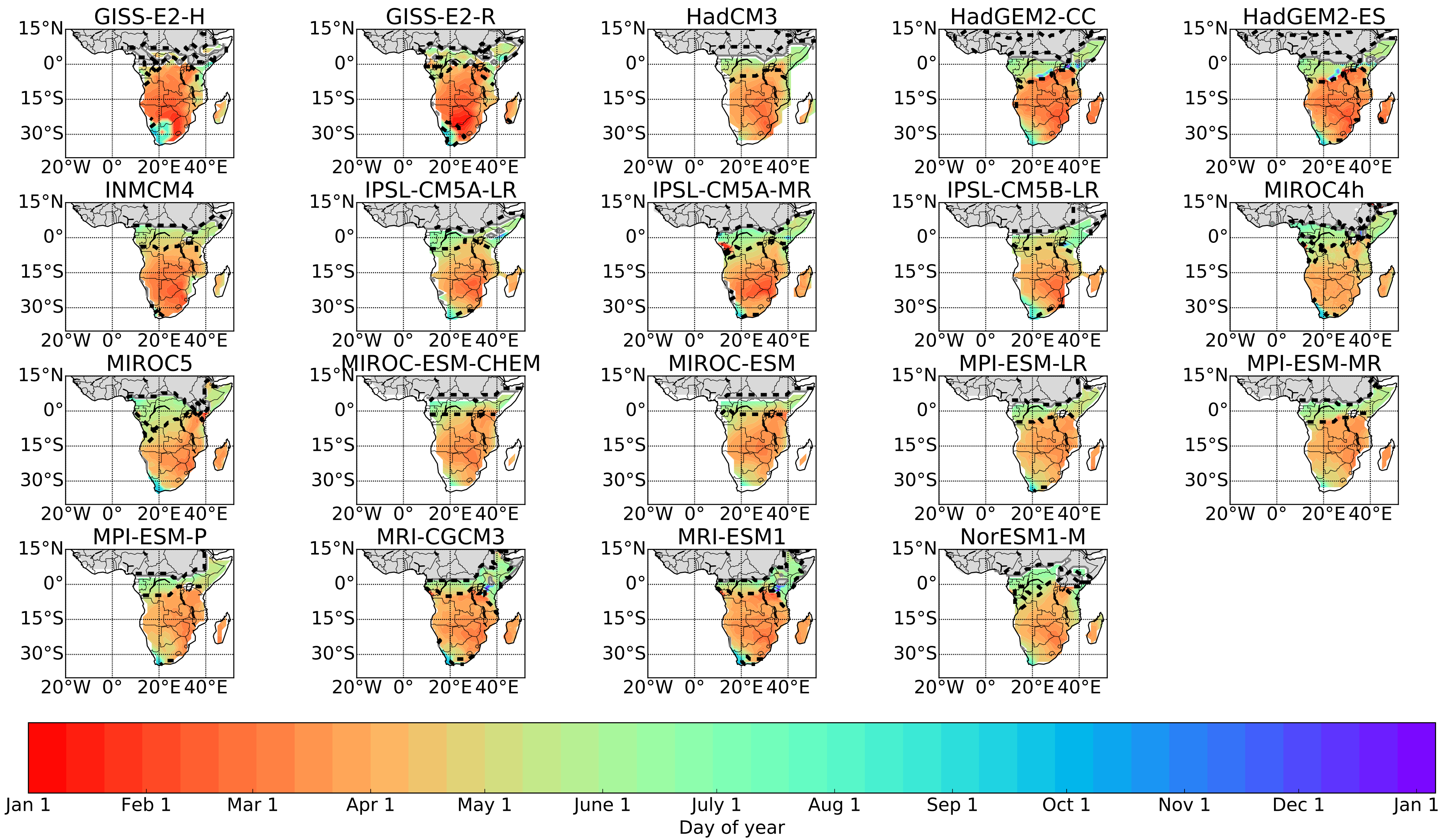

Figure S21: Seasonal progression of the onset/cessation of wet seasons in second half (alphabetical, first half in Fig S20) of the CMIP simulations used (Table S1). This plot shows the northward progression of cessation in boreal spring from the end of the annual rains over southern Africa into the first/long rains over then biannual regime region. The dashed black line shows the annual/biannual boundaries. Grey indicates regions not considered for these plots.

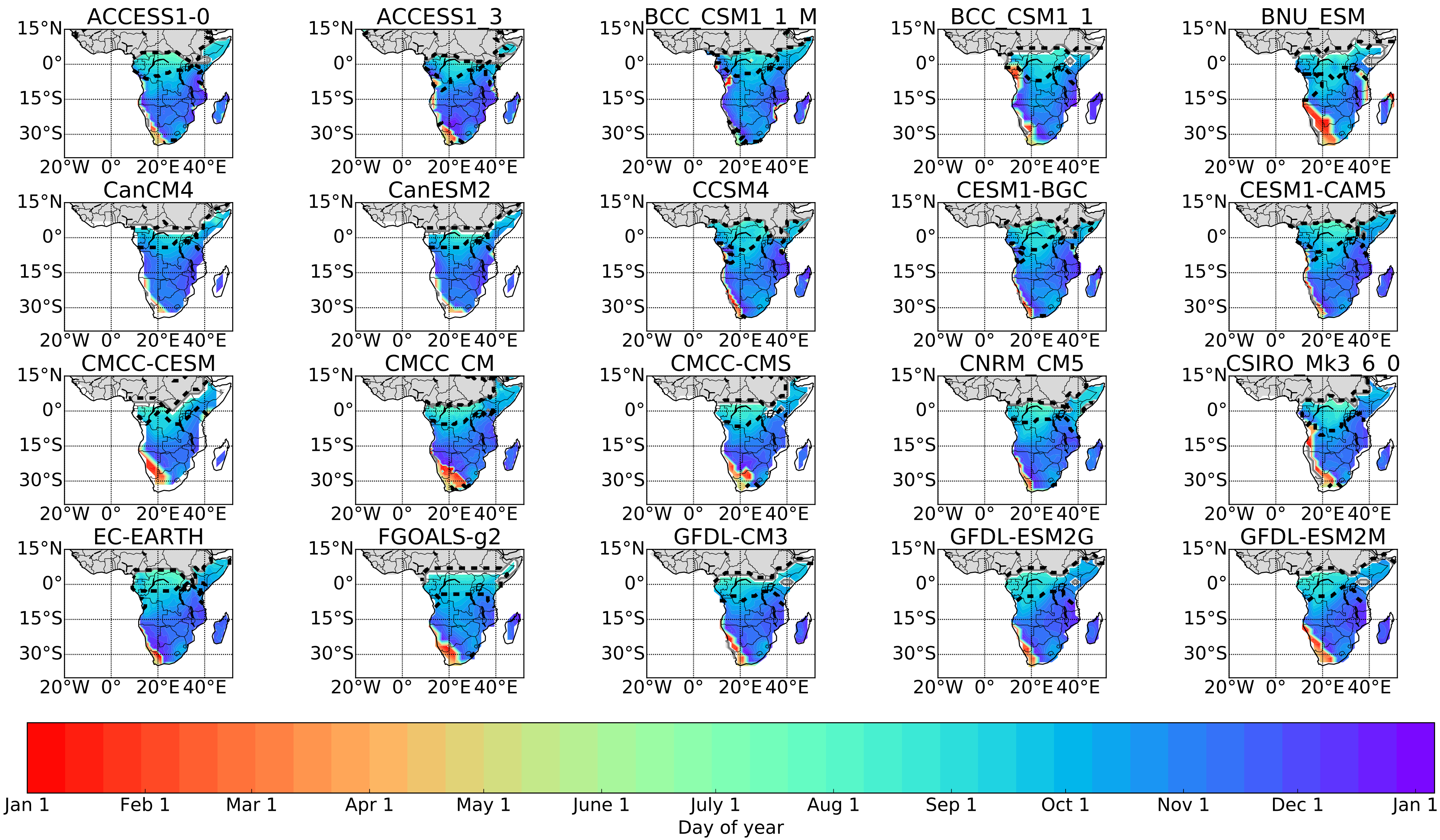

Figure S22: Seasonal progression of the onset/cessation of wet seasons in first half (alphabetical, second half in Fig S23) of the CMIP simulations used (Table S1). The southward progression of onset in boreal autumn is plotted, from the second/short rains over the biannual region into the annual rains over southern Africa. The dashed black line shows the annual/biannual boundaries. Grey indicates regions not considered for these plots.

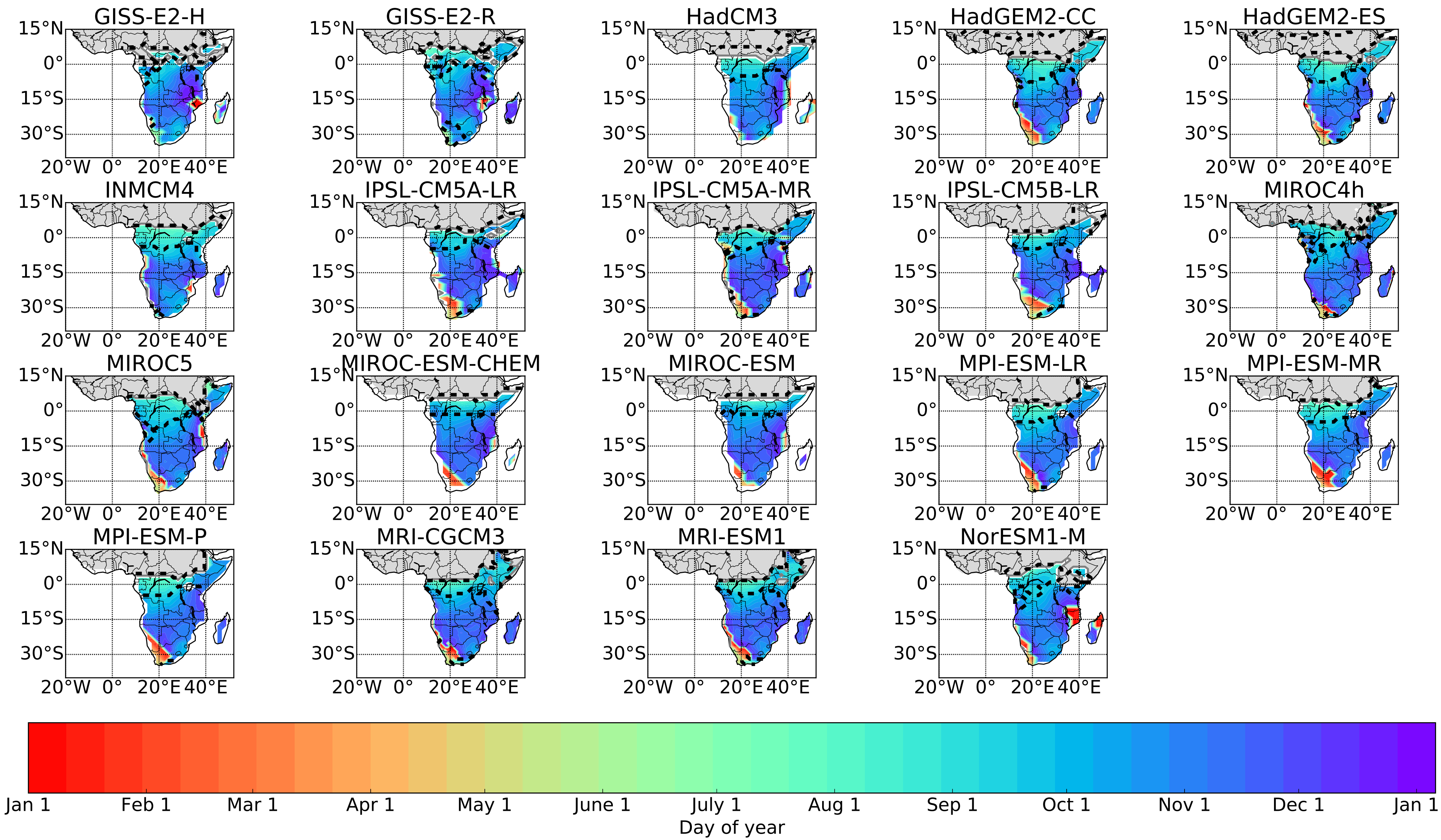

Figure S23: Seasonal progression of the onset/cessation of wet seasons in second half (alphabetical, first half in Fig S22) of the CMIP simulations used (Table S1). The southward progression of onset in boreal autumn is plotted, from the second/short rains over the biannual region into the annual rains over southern Africa. The dashed black line shows the annual/biannual boundaries. Grey indicates regions not considered for these plots.

References

Adachi, Y., S. Yukimoto, M. Deushi, A. Obata, H. Nakano, T. Y. Tanaka, M. Hosaka, T. Sakami, H. Yoshimura, M. Hirabara, et al. (2013), Basic performance of a new earth system model of the Meteorological Research Institute (MRI-ESM1), *Pap. Meteorol. Geophys*, *64*, 1–18.

Arora, V., J. Scinocca, G. Boer, J. Christian, K. Denman, G. Flato, V. Kharin, W. Lee, and W. Merryfield (2011), Carbon emission limits required to satisfy future representative concentration pathways of greenhouse gases, *Geophysical Research Letters*, *38*(5).

Bao, Q., P. Lin, T. Zhou, Y. Liu, Y. Yu, G. Wu, B. He, J. He, L. Li, J. Li, et al. (2013), The flexible global ocean-atmosphere-land system model, spectral version 2: FGOALS-s2, *Advances in Atmospheric Sciences*, *30*(3), 561–576.

Bi, D., M. Dix, S. J. Marsland, S. OFarrell, H. Rashid, P. Uotila, A. Hirst, E. Kowalczyk, M. Golebiewski, A. Sullivan, et al. (2013), The ACCESS coupled model: description, control climate and evaluation, *Aust. Meteorol. Oceanogr. J*, *63*(1), 41–64.

Collins, M., S. Tett, and C. Cooper (2001), The internal climate variability of HadCM3, a version of the Hadley Centre coupled model without flux adjustments, *Climate Dynamics*, *17*(1), 61–81.

Collins, W., N. Bellouin, M. Doutriaux-Boucher, N. Gedney, P. Halloran, T. Hinton, J. Hughes, C. Jones, M. Joshi, S. Liddicoat, et al. (2011), Development and evaluation of an Earth-System model-HadGEM2, *Geoscientific Model Development*, *4*(4), 1051.

Delworth, T. L., A. J. Broccoli, A. Rosati, R. J. Stouffer, V. Balaji, J. A. Beesley, W. F. Cooke, K. W. Dixon, J. Dunne, K. Dunne, et al. (2006), GFDL's CM2 global coupled climate models. Part I: Formulation and simulation characteristics, *Journal of Climate*, *19*(5), 643–674.

Dufresne, J.-L., M.-A. Foujols, S. Denvil, A. Caubel, O. Marti, O. Aumont, Y. Balkanski, S. Bekki, H. Bellenger, R. Benshila, et al. (2013), Climate change projections using the IPSL-CM5 Earth System Model: from CMIP3 to CMIP5, *Climate Dynamics*, *40*(9-10), 2123–2165.

Dunne, J. P., J. G. John, A. J. Adcroft, S. M. Griffies, R. W. Hallberg, E. Shevliakova, R. J. Stouffer, W. Cooke, K. A. Dunne, M. J. Harrison, et al. (2012), GFDLs ESM2 global coupled climate–carbon earth system models. Part I: Physical formulation and baseline simulation characteristics, *Journal of Climate*, *25*(19), 6646–6665.

Dunning, C. M., E. C. Black, and R. P. Allan (2016), The onset and cessation of seasonal rainfall over Africa, *Journal of Geophysical Research: Atmospheres*, *121*(19).

Fogli, P. G., E. Manzini, M. Vichi, A. Alessandri, L. Patara, S. Gualdi, E. Scoccimarro, S. Masina, and A. Navarra (2009), INGV-CMCC carbon (ICC): a carbon cycle earth system model.

Funk, C. C., P. J. Peterson, M. F. Landsfeld, D. H. Pedreros, J. P. Verdin, J. D. Rowland, B. E. Romero, G. J. Husak, J. C. Michaelsen, A. P. Verdin, et al. (2014), A quasi-global precipitation time series for drought monitoring, *US Geological Survey Data Series*, *832*(4).

Gent, P. R., G. Danabasoglu, L. J. Donner, M. M. Holland, E. C. Hunke, S. R. Jayne, D. M. Lawrence, R. B. Neale, P. J. Rasch, M. Vertenstein, et al. (2011), The community climate system model version 4, *Journal of Climate*, *24*(19), 4973–4991.

Hazeleger, W., X. Wang, C. Severijns, S. Ştefănescu, R. Bintanja, A. Sterl, K. Wyser, T. Semmler, S. Yang, B. Van den Hurk, et al. (2012), EC-Earth V2. 2: description and validation of a new seamless earth system prediction model, *Climate dynamics*, *39*(11), 2611–2629.

Huffman, G. J., R. F. Adler, M. M. Morrissey, D. T. Bolvin, S. Curtis, R. Joyce, B. McGavock, and J. Susskind (2001), Global precipitation at one-degree daily resolution from multisatellite observations, *Journal of Hydrometeorology*, *2*(1), 36–50.

Huffman, G. J., D. T. Bolvin, E. J. Nelkin, D. B. Wolff, R. F. Adler, G. Gu, Y. Hong, K. P. Bowman, and E. F. Stocker (2007), The TRMM multisatellite precipitation analysis (TMPA): Quasi-global, multiyear, combined-sensor precipitation estimates at fine scales, *Journal of Hydrometeorology*, *8*(1), 38–55.

	West Africa			Sahel			Central Africa		Southern Africa				
	1	2	3	5	6	7	10	11	12	13	14	15	16
OBS MEAN	150.8	130.5	129.4	155.4	116.3	142.4	285.2	329.7	329.6	307.6	317.0	287.7	351.5
OBS STD	3.4	3.7	4.2	3.5	4.5	6.2	3.7	3.4	2.1	4.7	2.1	14.7	3.0
AMIP_ACCESS1_0	-4	-24	-21	-35	-29	-31	-1	-7	3	0	3	-32	-22
AMIP_ACCESS1_3	1	-1	8	-10	5	8	13	-4	4	4	0	0	-20
AMIP_BCC_CSM1_1	-1	-9	-5	-31	×	-48	20	0	14	2	-6	-22	-19
AMIP_BCC_CSM1_1_M	0	-5	-9	-35	-20	-23	-1	-11	6	-4	-13	13	-28
AMIP_BNU_ESM	0	-5	-10	-24	×	34	-15	-10	-4	-41	-13	-59	9
AMIP_CCSM4	4	-4	-7	-32	-5	1	8	11	7	0	-10	2	-22
AMIP_CMCC-CM	1	11	0	8	-4	-7	8	-12	-11	1	-1	-6	-8
AMIP_CNRM_CM5	6	2	-24	-35	-25	-19	-1	-18	-7	-1	-7	-4	-22
AMIP_CSIRO_Mk3_6_0	8	7	-10	-36	-20	-35	22	8	1	-19	-4	-77	-1
AMIP_CanAM4	-2	-9	-22	-34	-10	8	12	-14	0	1	-10	0	-44
AMIP_FGOALS-g2	15	3	-9	-34	-17	-3	12	-9	-7	-10	-18	-6	-48
AMIP_FGOALS-s2	20	-20	-5	-47	-9	40	-7	-21	-9	-12	-2	12	5
AMIP_GFDL-CM3	-9	-21	-20	-25	-13	13	16	-7	5	15	0	-11	-12
AMIP_GFDL-HIRAM-C180	10	11	-2	-34	-15	-26	-3	-5	-5	-11	-3	-17	-9
AMIP_GFDL-HIRAM-C360	2	4	0	-22	-9	-10	-2	-15	-9	-16	-7	-5	-6
AMIP_GISS-E2-R	-9	-4	-15	-34	-16	11	10	0	21	4	0	-23	-43
AMIP_HadGEM2-A	-17	-27	-27	-39	-22	-34	-10	-15	0	-5	1	-23	-32
AMIP_INMCM4	20	29	13	-8	15	18	0	-15	11	24	3	4	-17
AMIP_IPSL-CM5A-LR	10	19	16	3	-1	17	16	16	6	14	4	1	-3
AMIP_IPSL-CM5A-MR	14	22	20	4	0	10	20	0	8	7	0	4	-3
AMIP_IPSL-CM5B-LR	3	0	-2	-9	7	38	-2	4	11	10	4	-38	-10
AMIP_MIROC5	1	0	-9	-19	-17	-8	5	6	1	-17	-5	-9	-32
AMIP_MPI-ESM-LR	0	1	-5	0	-3	-12	14	0	-5	3	0	-7	-11
AMIP_MPI-ESM-MR	2	1	-1	-6	-7	-15	14	0	-4	1	-6	-21	-13
AMIP_MRI-AGCM3-2H	2	-4	-19	-33	-21	-21	1	-8	-5	0	-7	7	-14
AMIP_MRI-AGCM3-2S	-3	-6	-17	-30	-23	-16	6	-2	-3	-12	-12	-18	-17
AMIP_MRI-CGCM3	-1	-9	-3	-22	-7	9	9	-1	-2	4	-8	-27	-32
AMIP_NorESM1_M	8	3	8	-17	-8	36	13	14	13	-16	-11	13	-19
AMIP DIFF MEAN	3.0	-1.3	-6.5	-23.1	-10.9	-2.4	6.4	-4.3	1.4	-2.6	-4.8	-12.7	-18.0
AMIP STD	8.6	13.0	12.1	14.9	10.6	23.6	9.8	9.8	8.3	13.0	6.1	20.8	14.1
CMIP_ACCESS1-0	4	-28	-24	-39	-27	1	-16	-18	0	0	-2	-38	-13
CMIP_ACCESS1_3	-2	-17	-6	-19	11	29	0	-23	4	8	12	-29	-11
CMIP_BCC_CSM1_1_M	20	9	-8	-30	-16	-3	0	-27	0	-5	-7	-1	-31
CMIP_BCC_CSM1_1	4	1	-11	-35	-10	-25	-83	-31	-5	-30	-11	-54	-6
CMIP_BNU_ESM	-10	-18	-16	-23	-24	2	-16	-11	7	-19	-5	-81	13
CMIP_CanCM4	4	-4	-22	-41	-13	5	7	-21	1	8	0	10	-28
CMIP_CanESM2	6	-3	-18	-38	-14	-5	3	-19	1	9	0	-2	-20
CMIP_CCSM4	0	-10	-17	-41	-4	0	-10	-10	0	-18	-15	-5	-11
CMIP_CESM1-BGC	6	-13	-22	-45	-7	0	-5	-11	1	-13	-11	0	-15
CMIP_CESM1-CAM5	14	-10	-28	-44	-26	-20	-9	-11	1	-13	0	-14	-10
CMIP_CMCC-CESM	4	6	0	15	-12	29	-12	-26	-8	0	0	-76	8
CMIP_CMCC-CMS	18	12	1	-3	-1	12	-5	-22	-9	3	12	-92	9
CMIP_CMCC_CM	17	18	6	0	-1	8	-1	-15	-8	4	5	-132	16
CMIP_CNRM_CM5	16	5	-12	-31	-20	-11	-13	-19	-4	-5	-5	-22	-5
CMIP_CSIRO_Mk3_6_0	-2	-1	-19	-42	-17	-27	3	-10	-4	-51	-1	-61	-3
CMIP_EC-EARTH	-24	-12	-25	-19	-11	-7	-12	-19	-1	-1	1	-21	-4
CMIP_FGOALS-g2	9	-1	-22	-50	-28	-12	-9	-28	-14	-9	-15	-118	-6
CMIP_GFDL-CM3	-9	-18	-22	-29	-10	10	2	-19	-2	-1	0	-45	1
CMIP_GFDL-ESM2G	4	3	-10	-30	-7	-1	0	-3	5	0	0	-47	-5
CMIP_GFDL-ESM2M	6	7	-7	-31	-6	-1	1	-5	11	2	1	-45	0
CMIP_GISS-E2-H	-25	-13	-14	-28	20	53	-4	2	-6	6	0	-59	-27
CMIP_GISS-E2-R	-23	-13	-14	-35	0	35	-5	0	18	5	3	-47	-31
CMIP_HadCM3	11	-11	-32	-55	-30	-39	-6	-11	-17	-12	-10	-26	-28
CMIP_HadGEM2-CC	14	-7	-6	-17	-17	-7	-18	-28	-9	-7	-5	-69	-1
CMIP_HadGEM2-ES	18	-5	-5	-14	-11	-9	-11	-29	-11	-4	-1	-20	-11
CMIP_INMCM4	-10	-24	-29	-51	-29	10	-6	-43	-5	16	1	-6	-24
CMIP_IPSL-CM5A-LR	15	23	8	-9	7	25	13	2	13	11	7	-61	7
CMIP_IPSL-CM5A-MR	16	30	17	-5	7	37	17	3	10	-2	7	-24	0
CMIP_IPSL-CM5B-LR	27	24	20	2	25	18	11	-12	0	10	-3	-100	3
CMIP_MIROC-ESM	-10	-15	-19	-12	-17	4	10	-5	1	8	7	-58	0
CMIP_MIROC-ESM-CHEM	-13	-16	-23	-16	-17	5	11	-7	17	9	3	-97	2
CMIP_MIROC4h	11	9	-6	-23	-7	9	-2	-11	5	-4	-1	-28	-20
CMIP_MIROC5	0	8	-7	-25	-17	-18	4	-11	8	0	-1	-38	-14
CMIP_MPI-ESM-LR	5	7	0	2	-4	6	-12	-13	-11	-8	-4	-58	3
CMIP_MPI-ESM-MR	8	11	1	1	-3	-7	-8	-11	-12	0	2	-50	8
CMIP_MPI-ESM-P	4	11	-1	3	-2	0	-11	-11	-8	0	-1	-95	5
CMIP_MRI-CGCM3	-4	-8	-4	-26	-6	-14	2	-26	-9	7	5	-47	-1
CMIP_MRI-ESM1	-4	-10	-6	-26	-6	-16	1	-24	-6	11	4	-80	-3
CMIP_NorESM1-M	-9	-18	-22	-43	-2	2	2	-2	12	-2	-6	-25	-7
CMIP DIFF MEAN	3.1	-2.4	-11.2	-24.8	-9.5	2.0	-4.9	-15.4	-0.9	-2.3	-0.9	-48.2	-6.9
CMIP STD	12.7	14.1	12.3	17.5	12.5	18.6	15.5	10.4	8.8	12.6	6.5	34.0	12.6

Figure S24: Figure showing the difference between the mean onset date over each region (Figure S1) for each simulation and the multi-observation mean onset for each region. The top two rows contain the multi-observation mean onset and standard deviation for each region. Negative numbers indicate an early onset, while positive numbers indicate a late onset. The dark red rows in the middle and at the bottom show the mean difference and standard deviation across the atmosphere-only and coupled simulations respectively. Yellow shading indicates the model mean is within the range of the five observational long term means for that region. Orange/ pale blue shading indicates the mean model onset date is within the observational interannual range (based on interannual standard deviation for each observational data set), and is early/ late respectively. Red/ dark blue shading indicates the mean model onset date is outside the observational range, and is early/ late respectively.

	West Africa			Sahel			Central Africa		Southern Africa				
	1	2	3	5	6	7	10	11	12	13	14	15	16
OBS MEAN	287.5	277.0	279.8	273.6	297.7	265.3	470.2	468.4	449.9	447.7	438.7	409.7	449.9
OBS STD	2.6	1.3	1.9	2.1	2.7	4.8	4.8	1.9	2.4	4.1	4.2	15.3	6.3
AMIP_ACCESS1_0	-12	3	-11	-7	0	8	-7	-9	-3	-2	-8	-24	-6
AMIP_ACCESS1_3	-11	-10	-4	-7	-1	20	-2	-1	2	0	-5	0	-3
AMIP_BCC_CSM1_1	1	-12	-12	-8	×	-13	-3	-9	0	0	2	-11	-2
AMIP_BCC_CSM1_1_M	-1	-1	-3	-4	-14	12	-21	-2	13	-2	-4	21	-7
AMIP_BNU_ESM	10	11	7	19	×	35	-3	-3	15	-19	7	-41	13
AMIP_CCSM4	9	7	4	14	9	24	0	-3	11	4	-1	21	1
AMIP_CMCC-CM	8	9	3	0	0	-2	6	-7	-6	1	5	-1	-3
AMIP_CNRM_CM5	3	7	0	0	-21	3	-12	2	11	4	6	16	9
AMIP_CSIRO_Mk3_6_0	3	15	11	1	-9	-17	0	-13	0	-13	5	-75	4
AMIP_CanAM4	-2	0	-6	-10	-14	6	-2	-6	-1	-2	-8	8	-5
AMIP_FGOALS-g2	8	13	9	13	-1	11	2	1	6	4	10	34	6
AMIP_FGOALS-s2	0	14	12	8	5	20	-23	6	10	-7	11	23	14
AMIP_GFDL-CM3	0	5	6	9	6	23	7	8	9	8	0	10	4
AMIP_GFDL-HIRAM-C180	1	-4	-13	-13	-12	-5	-9	-5	-1	-8	1	-6	3
AMIP_GFDL-HIRAM-C360	-3	-4	-10	-6	-6	2	-11	-4	0	-10	3	1	8
AMIP_GISS-E2-R	6	8	7	-7	-14	12	-8	0	17	-18	-16	-18	-29
AMIP_HadGEM2-A	-6	3	-12	-6	-6	-1	-16	-15	-2	-6	-9	-17	-9
AMIP_INMCM4	2	11	8	6	-1	33	-14	0	16	-6	0	15	-5
AMIP_IPSL-CM5A-LR	9	15	12	14	8	18	7	5	4	8	-5	0	2
AMIP_IPSL-CM5A-MR	5	14	12	13	7	13	10	-24	6	-1	-6	8	0
AMIP_IPSL-CM5B-LR	-5	-4	-12	-12	-11	-3	-32	1	-2	-5	-15	-48	-11
AMIP_MIROC5	4	5	0	-4	-9	2	4	0	4	-7	-3	12	5
AMIP_MPI-ESM-LR	3	2	-5	-3	-4	3	1	-11	0	5	6	5	2
AMIP_MPI-ESM-MR	3	2	-5	-4	-5	-1	-1	-11	0	-3	6	-5	-8
AMIP_MRI-AGCM3-2H	1	0	-9	-7	-7	-7	0	-13	-4	-2	-4	12	-3
AMIP_MRI-AGCM3-2S	1	0	-10	-6	-11	-12	4	-8	-7	-15	-8	-7	-6
AMIP_MRI-CGCM3	-8	-8	-17	-10	-12	6	-12	-11	-8	-7	-8	-16	-2
AMIP_NorESM1_M	3	6	1	14	15	41	2	5	18	-15	2	37	7
AMIP DIFF MEAN	1.3	4.0	-1.4	-0.3	-4.3	8.5	-4.9	-4.7	3.8	-4.2	-1.2	-1.7	-0.9
AMIP STD	6.0	7.8	9.3	9.8	8.9	14.7	10.2	7.6	7.9	7.7	7.3	24.5	8.8
CMIP_ACCESS1-0	-10	-5	-15	-12	-7	27	-21	-20	2	-3	-8	-34	-8
CMIP_ACCESS1_3	-18	-22	-19	-13	0	27	-7	-19	6	7	6	-27	4
CMIP_BCC_CSM1_1_M	11	11	-12	-8	-7	10	-15	5	13	-2	-9	0	-13
CMIP_BCC_CSM1_1	-4	-10	-11	-2	-4	9	-111	-24	-1	-30	-6	-49	10
CMIP_BNU_ESM	-2	-5	3	5	16	15	1	-1	13	5	1	-60	16
CMIP_CanCM4	-1	-2	-8	-12	-13	15	-1	-21	-3	0	-3	27	4
CMIP_CanESM2	2	1	-1	-10	-3	9	-2	-14	-6	-3	-7	-1	-1
CMIP_CCSM4	3	0	2	8	11	22	-15	-16	10	-13	0	19	7
CMIP_CESM1-BGC	2	4	4	7	9	15	-6	-14	12	-4	4	30	11
CMIP_CESM1-CAM5	5	1	3	11	7	23	-12	-9	13	-9	4	6	9
CMIP_CMCC-CESM	6	17	10	10	11	34	0	-5	4	5	4	-79	11
CMIP_CMCC-CMS	5	10	8	9	9	28	-1	-11	3	11	17	-96	17
CMIP_CMCC_CM	5	10	4	9	7	18	4	-5	3	5	16	-136	20
CMIP_CNRM_CM5	2	2	-2	1	-11	3	-7	2	20	12	16	-5	20
CMIP_CSIRO_Mk3_6_0	-2	0	-8	-4	-4	-4	-4	-11	0	-49	-3	-64	2
CMIP_EC-EARTH	-6	2	3	4	2	12	-8	-18	3	0	17	3	20
CMIP_FGOALS-g2	0	10	10	10	-2	14	0	6	18	12	17	-92	28
CMIP_GFDL-CM3	2	11	12	14	8	27	2	-9	10	6	6	-29	20
CMIP_GFDL-ESM2G	7	12	10	1	2	12	-8	-6	16	5	3	-28	12
CMIP_GFDL-ESM2M	6	13	11	2	2	12	-8	-10	14	5	2	-40	11
CMIP_GISS-E2-H	-2	3	3	-7	9	35	-24	-11	-11	-22	-17	-57	-22
CMIP_GISS-E2-R	4	7	4	-3	-3	23	-19	-9	7	-22	-22	-48	-22
CMIP_HadCM3	-3	1	-3	-10	0	8	-6	-6	-18	0	0	-5	5
CMIP_HadGEM2-CC	-6	-5	-22	-19	-2	8	-45	-32	-7	-10	-12	-67	5
CMIP_HadGEM2-ES	-8	-7	-16	-16	-3	7	-41	-32	-10	-12	-13	-22	-3
CMIP_INMCM4	-3	3	-3	-1	-5	23	-12	-9	5	-9	-2	8	-14
CMIP_IPSL-CM5A-LR	4	9	13	8	7	18	10	3	6	4	-6	-66	11
CMIP_IPSL-CM5A-MR	6	4	16	12	8	27	9	0	4	-16	-14	-33	-7
CMIP_IPSL-CM5B-LR	-2	0	-9	-17	-4	-13	5	9	8	8	-3	-97	14
CMIP_MIROC-ESM	-8	2	4	6	4	24	0	-19	-14	-1	15	-38	15
CMIP_MIROC-ESM-CHEM	-9	1	4	7	5	25	0	-16	7	0	7	-85	13
CMIP_MIROC4h	-4	-1	-1	-2	5	17	15	4	22	11	12	-23	2
CMIP_MIROC5	3	1	0	-3	-6	0	11	-12	5	12	1	-26	9
CMIP_MPI-ESM-LR	5	10	8	5	6	6	-5	-15	-1	3	16	-48	19
CMIP_MPI-ESM-MR	4	8	6	5	2	5	-9	-19	-1	7	17	-40	19
CMIP_MPI-ESM-P	6	9	6	6	6	-1	-5	-19	0	6	13	-88	20
CMIP_MRI-CGCM3	-8	1	-5	-8	-8	4	-17	-27	0	-1	1	-43	4
CMIP_MRI-ESM1	-11	-2	-11	-10	-8	1	-21	-26	0	1	0	-80	7
CMIP_NorESM1-M	-1	0	2	2	11	29	2	-2	8	12	7	1	18
CMIP DIFF MEAN	-0.5	3.0	0.1	-0.4	1.5	15.1	-9.5	-11.6	4.2	-1.7	2.1	-39.0	7.9
CMIP STD	6.5	7.4	9.6	9.4	7.3	11.1	20.7	10.5	9.3	12.9	10.8	38.3	12.0

Figure S25: Figure showing the difference between the mean cessation date over each region (Figure S1) for each simulation and the multi-observation mean cessation for each region. The top two rows contain the multi-observation mean cessation and standard deviation for each region. Negative numbers indicate an early cessation, while positive numbers indicate a late cessation. The dark red rows in the middle and at the bottom show the mean difference and standard deviation across the atmosphere-only and coupled simulations respectively. Yellow shading indicates the model mean is within the range of the five observational long term means for that region. Orange/ pale blue shading indicates the mean model cessation date is within the observational interannual range (based on interannual standard deviation for each observational data set), and is early/ late respectively. Red/ dark blue shading indicates the mean model cessation date is outside the observational range, and is early/ late respectively.

	Long Rains		Short Rains	
	Onset	End	Onset	End
OBS MEAN	97.2	135.8	279.5	313.0
OBS STD	3.3	2.3	4.2	3.2
AMIP_ACCESS1_0	-3	8	0	15
AMIP_ACCESS1_3	0	9	6	28
AMIP_BCC_CSM1_1	-9	-2	11	4
AMIP_BCC_CSM1_1_M	-11	10	-17	10
AMIP_BNU_ESM	1	21	1	26
AMIP_CCSM4	7	15	-3	20
AMIP_CMCC-CM	-13	-7	5	-1
AMIP_CNRM_CM5	0	17	-9	14
AMIP_CSIRO_Mk3_6_0	-4	2	9	18
AMIP_CanAM4	2	3	-17	12
AMIP_FGOALS-g2	1	12	15	23
AMIP_FGOALS-s2	-23	2	3	31
AMIP_GFDL-CM3	0	8	-2	30
AMIP_GFDL-HIRAM-C180	-15	-1	9	13
AMIP_GFDL-HIRAM-C360	-14	-4	5	16
AMIP_GISS-E2-R	-16	10	7	27
AMIP_HadGEM2-A	-4	4	0	14
AMIP_INMCM4	-4	-2	-13	38
AMIP_IPSL-CM5A-LR	12	19	-6	-1
AMIP_IPSL-CM5A-MR	31	33	-13	-8
AMIP_IPSL-CM5B-LR	1	-1	18	20
AMIP_MIROC5	16	27	1	17
AMIP_MPI-ESM-LR	-20	-12	11	6
AMIP_MPI-ESM-MR	-16	-6	16	9
AMIP_MRI-AGCM3-2H	-14	-4	-2	11
AMIP_MRI-AGCM3-2S	-19	-1	1	11
AMIP_MRI-CGCM3	0	2	15	17
AMIP_NorESM1_M	5	22	0	21
AMIP DIFF MEAN	-4.0	6.7	1.9	16.1
AMIP STD	12.2	11.1	10.0	10.5
CMIP_ACCESS1-0	30	19	-22	-1
CMIP_ACCESS1_3	45	35	-22	1
CMIP_BCC_CSM1_1_M	-6	17	-11	16
CMIP_BCC_CSM1_1	26	14	-11	15
CMIP_BNU_ESM	30	21	-5	30
CMIP_CanCM4	16	7	-11	16
CMIP_CanESM2	6	1	-5	13
CMIP_CCSM4	37	26	-13	24
CMIP_CESM1-BGC	43	32	-7	28
CMIP_CESM1-CAM5	20	24	-2	26
CMIP_CMCC-CESM	-8	0	2	26
CMIP_CMCC-CMS	13	-4	-6	24
CMIP_CMCC_CM	16	3	-5	17
CMIP_CNRM_CM5	12	13	-23	15
CMIP_CSIRO_Mk3_6_0	3	0	8	2
CMIP_EC-EARTH	-1	4	-9	13
CMIP_FGOALS-g2	12	22	-31	26
CMIP_GFDL-CM3	31	15	-17	22
CMIP_GFDL-ESM2G	26	14	4	23
CMIP_GFDL-ESM2M	33	19	2	20
CMIP_GISS-E2-H	35	47	-12	32
CMIP_GISS-E2-R	11	21	-4	31
CMIP_HadCM3	6	15	-7	21
CMIP_HadGEM2-CC	23	8	-22	-1
CMIP_HadGEM2-ES	23	7	-19	-3
CMIP_INMCM4	5	3	-35	17
CMIP_IPSL-CM5A-LR	27	26	3	19
CMIP_IPSL-CM5A-MR	13	13	6	20
CMIP_IPSL-CM5B-LR	40	35	0	8
CMIP_MIROC-ESM	22	19	-23	23
CMIP_MIROC-ESM-CHEM	25	26	-25	15
CMIP_MIROC4h	16	20	0	25
CMIP_MIROC5	23	33	-12	-16
CMIP_MPI-ESM-LR	15	4	9	13
CMIP_MPI-ESM-MR	20	14	8	7
CMIP_MPI-ESM-P	15	6	12	13
CMIP_MRI-CGCM3	33	22	-22	1
CMIP_MRI-ESM1	34	24	-23	0
CMIP_NorESM1-M	48	35	-8	36
CMIP DIFF MEAN	21.4	17.3	-9.4	16.3
CMIP STD	13.6	11.8	12.0	11.5

Figure S26: Figure showing the difference between the mean onset and cessation dates over the Horn of Africa (Figure S1) for each simulation and the multi-observation mean onset and cessation dates, for each season. The top two rows contain the multi-observation mean onset/cessation and standard deviation for each season. Negative numbers indicate an early onset/cessation, while positive numbers indicate a late onset/cessation. The dark red rows in the middle and at the bottom show the mean difference and standard deviation across the atmosphere-only and coupled simulations respectively. Yellow shading indicates the model mean is within the range of the five observational long term means for that region. Orange/ pale blue shading indicates the mean model onset or cessation date is within the observational interannual range (based on interannual standard deviation for each observational data set), and is early/ late respectively. Red/ dark blue shading indicates the mean model onset or cessation date is outside the observational range, and is early/ late respectively.

Table S1: List of models and institutions that provided model output used in this study. Where AMIP and CMIP (historical) simulations have been used for a certain model, the period used is indicated. A cross indicates that simulation was not used. Horizontal resolution and references for each model are also included. * Monthly SST data was not available for these models, and they are not included in Figure 5.

Institute	Model	AMIP	CMIP (Historical)	Resolution (Lat° x Lon°)	Reference
CSIRO-BOM	ACCESS 1.0	1979-2008	1979-2005	1.25 x 1.875	*Bi et al.* (2013)
CSIRO-BOM	ACCESS 1.3	1978-2008	1979-2005	1.25 x 1.875	*Bi et al.* (2013)
BCC	BCC-CSM1-1	1979-2008	1979-2005	2.78 x 2.81	*Wu, T and others* (2012)
BCC	BCC-CSM1-1-M	1979-2008	1979-2005	1.12 x 1.125	*Wu, T and others* (2012)
BNU	BNU-ESM*	1979-2008	1979-2005	2.78 x 2.813	*Ji et al.* (2014)
CCCma	CanAM4	1979-2009	x	2.77 x 2.813	*Arora et al.* (2011)
CCCma	CanCM4	x	1979-2005	2.79 x 2.813	*Arora et al.* (2011)
CCCma	CanESM2	x	1979-2005	2.79 x 2.813	*Arora et al.* (2011)
NCAR	CCSM4	1979-2010	1979-2005	0.94 x 1.25	*Gent et al.* (2011)
NSF-DOE-NCAR	CESM1-BGC	x	1979-2005	0.94 x 1.25	*Long et al.* (2013)
NSF-DOE-NCAR	CESM1-CAM5	x	1979-2005	0.94 x 1.25	*Hurrell et al.* (2013)
CMCC	CMCC-CM	1979-2008	1979-2005	0.74 x 0.75	*Fogli et al.* (2009)
CMCC	CMCC-CESM	x	1979-2005	3.71 x 3.75	*Fogli et al.* (2009)
CMCC	CMCC-CMS	x	1979-2005	1.87 x 1.875	*Fogli et al.* (2009)
CNRM-CERFACS	CNRM-CM5	1979-2008	1979-2005	1.40 x 1.406	*Voldoire et al.* (2013)
CSIRO-QCCCE	CSIRO-Mk3-6-0	1979-2009	1979-2005	1.85 x 1.875	*Jeffrey et al.* (2013)
ICHEC	EC-EARTH	x	1979-2005	1.12 x 1.125	*Hazeleger et al.* (2012)
LASG-CESS	FGOALS-g2	1979-2008	1979-2005	2.79 x 2.813	*Li et al.* (2013)
LASG-IAP	FGOALS-s2	1979-2008	x	1.65 x 2.813	*Bao et al.* (2013)
NOAA-GFDL	GFDL-HIRAM-C180	1979-2008	x	0.50 x 0.625	*Delworth et al.* (2006)
NOAA-GFDL	GFDL-HIRAM-C360	1979-2008	x	0.25 x 0.325	*Delworth et al.* (2006)
NOAA-GFDL	GFDL-CM3	1979-2008	1979-2005	2.00 x 2.5	*Delworth et al.* (2006)
NOAA-GFDL	GFDL-ESM2G	x	1979-2005	2.02 x 2.5	*Dunne et al.* (2012)
NOAA-GFDL	GFDL-ESM2M	x	1979-2005	2.02 x 2.5	*Dunne et al.* (2012)
NASA-GISS	GISS-E2-H*	x	1979-2005	2.00 x 2.5	*Schmidt et al.* (2006)
NASA-GISS	GISS-E2-R	1979-2008	1979-2005	2.00 x 2.5	*Schmidt et al.* (2006)
MOHC	HadCM3	x	1979-2005	2.50 x 3.75	*Collins et al.* (2001)
MOHC	HadGEM2-A	1979-2008	x	1.25 x 1.875	*Collins et al.* (2011)
MOHC	HadGEM2-CC	x	1979-2004	1.25 x 1.875	*Collins et al.* (2011)
MOHC	HadGEM2-ES	x	1979-2004	1.25 x 1.875	*Collins et al.* (2011)
INM	INMCM4	1979-2008	1979-2005	1.50 x 2	*Volodin et al.* (2010)
IPSL	IPSL-CM5A-LR	1979-2009	1979-2005	1.89 x 3.75	*Dufresne et al.* (2013)
IPSL	IPSL-CM5A-MR	1979-2009	1979-2005	1.27 x 2.5	*Dufresne et al.* (2013)
IPSL	IPSL-CM5B-LR	1979-2008	1979-2005	1.89 x 3.75	*Dufresne et al.* (2013)
MIROC	MIROC4h	x	1979-2005	0.56 x 0.56	*Sakamoto et al.* (2012)
MIROC	MIROC5	1979-2008	1979-2005	1.40 x 1.406	*Watanabe et al.* (2010)
MIROC	MIROC-ESM	x	1979-2005	2.79 x 2.813	*Watanabe et al.* (2011)
MIROC	MIROC-ESM-CHEM	x	1979-2005	2.79 x 2.813	*Watanabe et al.* (2011)
MPI-M	MPI-ESM-LR	1979-2008	1979-2005	1.86 x 1.875	*Stevens et al.* (2013)
MPI-M	MPI-ESM-MR	1979-2008	1979-2005	1.86 x 1.875	*Stevens et al.* (2013)
MPI-M	MPI-ESM-P	x	1979-2005	1.86 x 1.875	*Stevens et al.* (2013)
MRI	MRI-AGCM3-2H	1979-2007	x	0.56 x 0.563	*Mizuta et al.* (2012)
MRI	MRI-AGCM3-2S	1979-2007	x	0.19 x 0.188	*Mizuta et al.* (2012)
MRI	MRI-CGCM3	1979-2008	1979-2005	1.12 x 1.125	*Yukimoto et al.* (2011)
MRI	MRI-ESM1	x	1979-2005	1.12 x 1.125	*Adachi et al.* (2013)
NCC	NorESM1-M	1979-2008	1979-2005	1.89 x 2.5	*Iversen et al.* (2012)

Table S2: Description of some of the characteristics of the observational datasets of African precipitation used in this study.

Data	Spatial Resolution	Period Used	Reference
TARCAT	0.0375°	1984-2014	*Maidment et al.* (2014)
ARC	0.1°	1983-2013	*Novella and Thiaw* (2013)
GPCP	1°	1997-2014	*Huffman et al.* (2001)
TRMM 3B42	0.25°	1998-2014	*Huffman et al.* (2007)
CHIRPS	0.05°	1981-2014	*Funk et al.* (2014)

Hurrell, J. W., M. M. Holland, P. R. Gent, S. Ghan, J. E. Kay, P. Kushner, J.-F. Lamarque, W. G. Large, D. Lawrence, K. Lindsay, et al. (2013), The community earth system model: a framework for collaborative research, *Bulletin of the American Meteorological Society*, *94*(9), 1339–1360.

Iversen, T., M. Bentsen, I. Bethke, J. Debernard, A. Kirkevåg, Ø. Seland, H. Drange, J. Kristjánsson, I. Medhaug, M. Sand, et al. (2012), The Norwegian earth system model, NorESM1-M–Part 2: Climate response and scenario projections, *Geosci. Model Dev. Discuss*, *5*(3), 2933–2998.

Jeffrey, S., L. Rotstayn, M. Collier, S. Dravitzki, C. Hamalainen, C. Moeseneder, K. Wong, and J. Syktus (2013), Australias CMIP5 submission using the CSIRO Mk3. 6 model, *Aust. Meteor. Oceanogr. J*, *63*, 1–13.

Ji, D., L. Wang, J. Feng, Q. Wu, H. Cheng, Q. Zhang, J. Yang, W. Dong, Y. Dai, D. Gong, et al. (2014), Description and basic evaluation of Beijing Normal University Earth system model (BNU-ESM) version 1, *Geoscientific Model Development*, *7*(5), 2039–2064.

Li, L., P. Lin, Y. Yu, B. Wang, T. Zhou, L. Liu, J. Liu, Q. Bao, S. Xu, W. Huang, et al. (2013), The flexible global ocean-atmosphere-land system model, Grid-point Version 2: FGOALS-g2, *Advances in Atmospheric Sciences*, *30*(3), 543–560.

Long, M. C., K. Lindsay, S. Peacock, J. K. Moore, and S. C. Doney (2013), Twentieth-century oceanic carbon uptake and storage in CESM1 (BGC), *Journal of Climate*, *26*(18), 6775–6800.

Maidment, R. I., D. Grimes, R. P. Allan, E. Tarnavsky, M. Stringer, T. Hewison, R. Roebeling, and E. Black (2014), The 30 year TAMSAT African Rainfall Climatology And Time series (TARCAT) data set, *Journal of Geophysical Research: Atmospheres*, *119*(18), 10–619.

Mizuta, R., H. Yoshimura, H. Murakami, M. Matsueda, O. Tomoaki, K. KAMIGUCHI, M. HOSAKA, S. Masato, S. YUKIMOTO, S. KUSUNOKI, et al. (2012), Climate simulations using mri-agcm3. 2 with 20-km grid, *Journal of the Meteorological Society of Japan. Ser. II*, *90*, 233–258.

Novella, N. S., and W. M. Thiaw (2013), African rainfall climatology version 2 for famine early warning systems, *Journal of Applied Meteorology and Climatology*, *52*(3), 588–606.

Sakamoto, T. T., Y. Komuro, T. Nishimura, M. Ishii, H. Tatebe, H. Shiogama, A. Hasegawa, T. Toyoda, T. SUZUKI, Y. IMADA, et al. (2012), MIROC4ha new high-resolution atmosphere-ocean coupled general circulation model, *Journal of the Meteorological Society of Japan. Ser. II*, *90*(3), 325–359.

Schmidt, G. A., R. Ruedy, J. E. Hansen, I. Aleinov, N. Bell, M. Bauer, S. Bauer, B. Cairns, V. Canuto, Y. Cheng, et al. (2006), Present-day atmospheric simulations using GISS ModelE: Comparison to in situ, satellite, and reanalysis data, *Journal of Climate*, *19*(2), 153–192.

Stevens, B., M. Giorgetta, M. Esch, T. Mauritsen, T. Crueger, S. Rast, M. Salzmann, H. Schmidt, J. Bader, K. Block, et al. (2013), Atmospheric component of the MPI-M Earth System Model: ECHAM6, *Journal of Advances in Modeling Earth Systems*, *5*(2), 146–172.

Voldoire, A., E. Sanchez-Gomez, D. S. y Mélia, B. Decharme, C. Cassou, S. Sénési, S. Valcke, I. Beau, A. Alias, M. Chevallier, et al. (2013), The CNRM-CM5. 1 global climate model: description and basic evaluation, *Climate Dynamics*, *40*(9-10), 2091–2121.

Volodin, E., N. Dianskii, and A. Gusev (2010), Simulating present-day climate with the INMCM4. 0 coupled model of the atmospheric and oceanic general circulations, *Izvestiya, Atmospheric and Oceanic Physics*, *46*(4), 414–431.

Watanabe, M., T. Suzuki, R. Oishi, Y. Komuro, S. Watanabe, S. Emori, T. Takemura, M. Chikira, T. Ogura, M. Sekiguchi, et al. (2010), Improved climate simulation by MIROC5: mean states, variability, and climate sensitivity, *Journal of Climate*, *23*(23), 6312–6335.

Watanabe, S., T. Hajima, K. Sudo, T. Nagashima, T. Takemura, H. Okajima, T. Nozawa, H. Kawase, M. Abe, T. Yokohata, et al. (2011), MIROC-ESM 2010: Model description and basic results of CMIP5-20c3m experiments, *Geoscientific Model Development*, *4*(4), 845.

Wu, T and others (2012), The 20th century global carbon cycle from the Beijing Climate Center Climate System Model (BCC CSM), *J Clim*.

Yukimoto, S., H. Yoshimura, M. Hosaka, T. Sakami, H. Tsujino, M. Hirabara, T. Tanaka, M. Deushi, A. Obata, H. Nakano, et al. (2011), Meteorological Research Institute Earth System Model Version 1 (MRI-ESM1): Model Description–Technical reports of the meteorological research institute No. 64, *Meteorological Research Institute, Japan*.